Supporting information

Cu(I) Complexes Obtained via Spontaneous Reduction of Cu(II) Complexes Supported by Designed Bidentate Ligands: Bioinspired Cu(I) Based Catalysts for Aromatic Hydroxylation

Sheela Kumari,[†,§] Sethuraman Muthuramalingam,[‡,§] Ashish Kumar Dhara[†], U. P. Singh[†], Ramasamy Mayilmurugan[*‡], Kaushik Ghosh[*†]

[†]Department of Chemistry, Indian Institute of Technology Roorkee, Roorkee -247667, INDIA, E-mail: kaushik.ghosh@cy.iitr.ac.in

[‡]Bioinorganic Chemistry Laboratory/Physical Chemistry, School of Chemistry, Madurai Kamaraj University, Madurai-625021, INDIA, E-mail: mayilmurugan.chem@mkuniversity.ac.in

[§]Both authors contributed equally to this manuscript.

Table of Contents

Figure S1. IR spectrum of ligand (L^1).
Figure S2. IR spectrum of ligand (L^2).
Figure S3. IR spectrum of ligand (L^3).
Figure S4. IR spectrum of ligand (L^4).
Figure S5. IR spectrum of ligand (L^5).
Figure S6. IR spectrum of ligand (L^6).
Figure S7. IR spectrum of ligand (L^7).
Figure S8. IR spectrum of complex **1**.
Figure S9. IR spectrum of complex **2**.
Figure S10. IR spectrum of complex **3**.
Figure S11. IR spectrum of complex **4**.
Figure S12. IR spectrum of complex **5**.
Figure S13. IR spectrum of complex **6**.
Figure S14. IR spectrum of complex **6**.
Figure S15. ^{1}H NMR spectrum of ligand (L^1).
Figure S16. ^{13}C NMR spectrum of ligand (L^1).
Figure S17. ^{1}H NMR spectrum of ligand (L^2).
Figure S18. ^{13}C NMR spectrum of ligand (L^2).
Figure S19. ^{1}H NMR spectrum of ligand (L^3).
Figure S20. ^{13}C NMR spectrum of ligand (L^3).
Figure S21. ^{1}H NMR spectrum of ligand (L^4).
Figure S22. ^{13}C NMR spectrum of ligand (L^4).
Figure S23. ^{1}H NMR spectrum of ligand (L^5).
Figure S24. ^{13}C NMR spectrum of ligand (L^5).
Figure S25. ^{1}H NMR spectrum of ligand (L^6).
Figure S26. ^{13}C NMR spectrum of ligand (L^6).
Figure S27. ^{1}H NMR spectrum of ligand (L^7).
Figure S28. ^{13}C NMR spectrum of ligand (L^7).
Figure S29. UV-visible spectra of ligands (L^1-L^7).
Figure S30. UV-visible spectra of complexes (**1-7**).
Figure S31. ^{1}H NMR spectrum of complex **1**.
Figure S32. ^{1}H NMR spectrum of complex **2**.
Figure S33. ^{1}H NMR spectrum of complex **3**.
Figure S34. ^{1}H NMR spectrum of complex **4**.
Figure S35. ^{1}H NMR spectrum of complex **5**.
Figure S36. ^{1}H NMR spectrum of complex **6**.
Figure S37. ^{1}H NMR spectrum of complex **7**.
Figure S38. HRMS spectrum of complex **1.**

Figure S39. HRMS spectrum of complex **2.**
Figure S40. HRMS spectrum of complex **3.**
Figure S41. HRMS spectrum of complex **4.**
Figure S42. HRMS spectrum of complex **5.**
Figure S43. HRMS spectrum of complex **6.**
Figure S44. HRMS spectrum of complex **7.**
Figure S45. Oxidation of ABTS during spontaneous reduction.
Figure S46. GC-MS profile for the formation of phenol using catalyst **7** and in presence of nitrobenzene as an internal standard.
Figure S47. (a) The plot of yield versus various concentration of complex. **(b)** H_2O_2 dependent on the yield of phenol.
Figure S48. GC trace for the oxidation of toluene using catalyst **7**.
Figure S49. GC trace for the oxidation of ethylbenzene using catalyst **7**.
Figure S50. GC trace for the oxidation of cumene using catalyst **7**.
Figure S51. GC trace for the oxidation of chlorobenzene using catalyst **7**.
Figure S52. GC trace for the oxidation of nitrobenzene using catalyst **7**.
Figure S53. GC-MS profile for the measurement of KIE using C_6H_6 and C_6D_6 and **7** is employed as catalyst.
Figure S54. HRMS spectrum of the formation of Cu(II)-species
Figure S55. The electronic spectral changes for the reaction of **1** with 10 equivalents of H_2O_2 and 2 equivalents of Et_3N in acetonitrile at -40 °C.
Figure S56. The electronic spectral changes for the reaction of **2** with 10 equivalents of H_2O_2 and 2 equivalents of Et_3N in acetonitrile at -40 °C.
Figure S57. The electronic spectral changes for the reaction of **4** with 10 equivalents of H_2O_2 and 2 equivalents of Et_3N in acetonitrile at -40 °C.
Figure S58. The electronic spectral changes for the reaction of **5** with 10 equivalents of H_2O_2 and 2 equivalents of Et_3N in acetonitrile at -40 °C.
Figure S59. GC trace of the benzene hydroxylation reaction in the presence of CCl_4 as additive using catalyst **7**.
Figure S60. Time depended phenol formation by **7**.
Table S1. NMR, IR and UV-Visible data of ligands (L^1-L^7).
Table S2. Bond parameters of complex **1**.
Table S3. Crystal data of complex **1**.
Table S4. Redox data of **1-7**.
Table S5. Optimization of benzene hydroxylation by **7**.

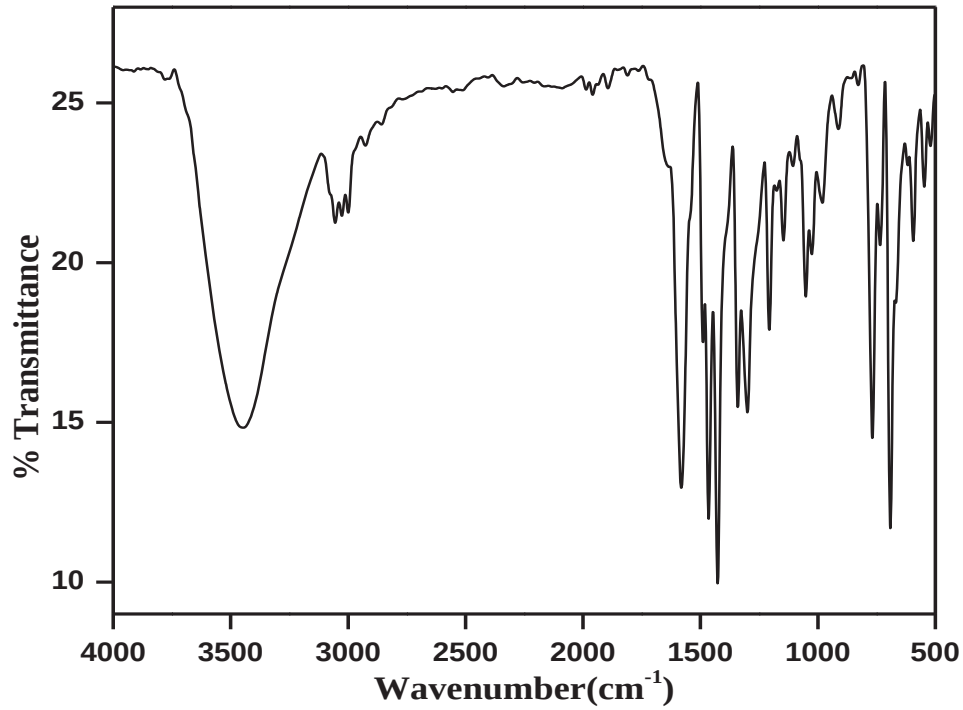

Figure S1. IR spectrum of ligand (L^1).

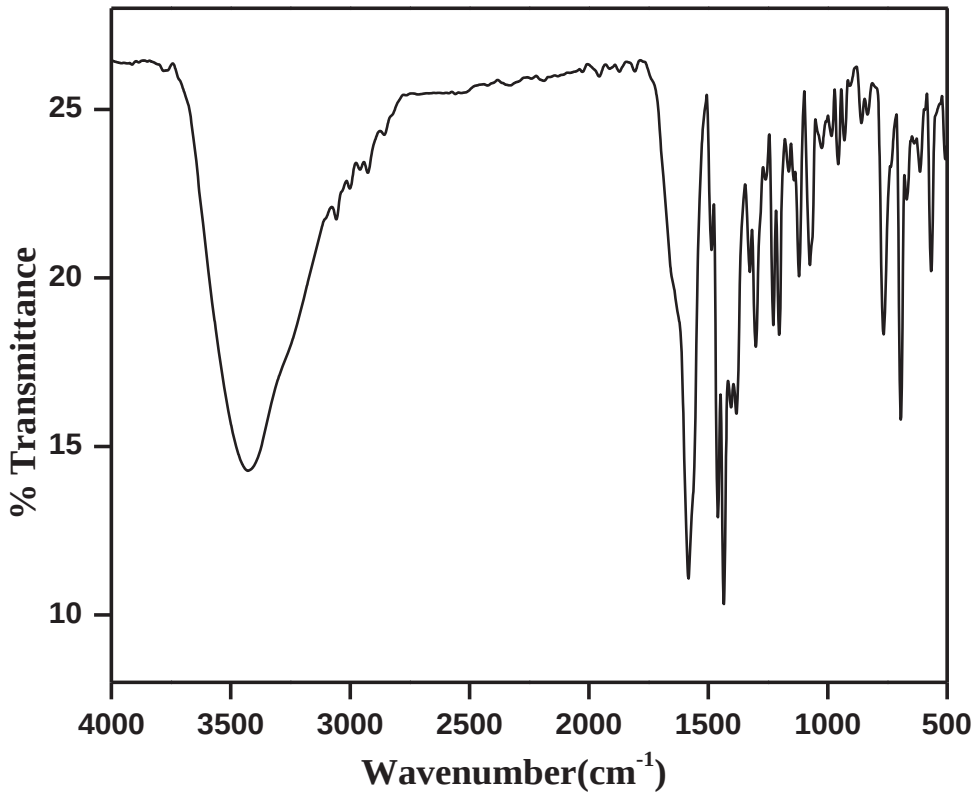

Figure S2. IR spectrum of ligand (L^2).

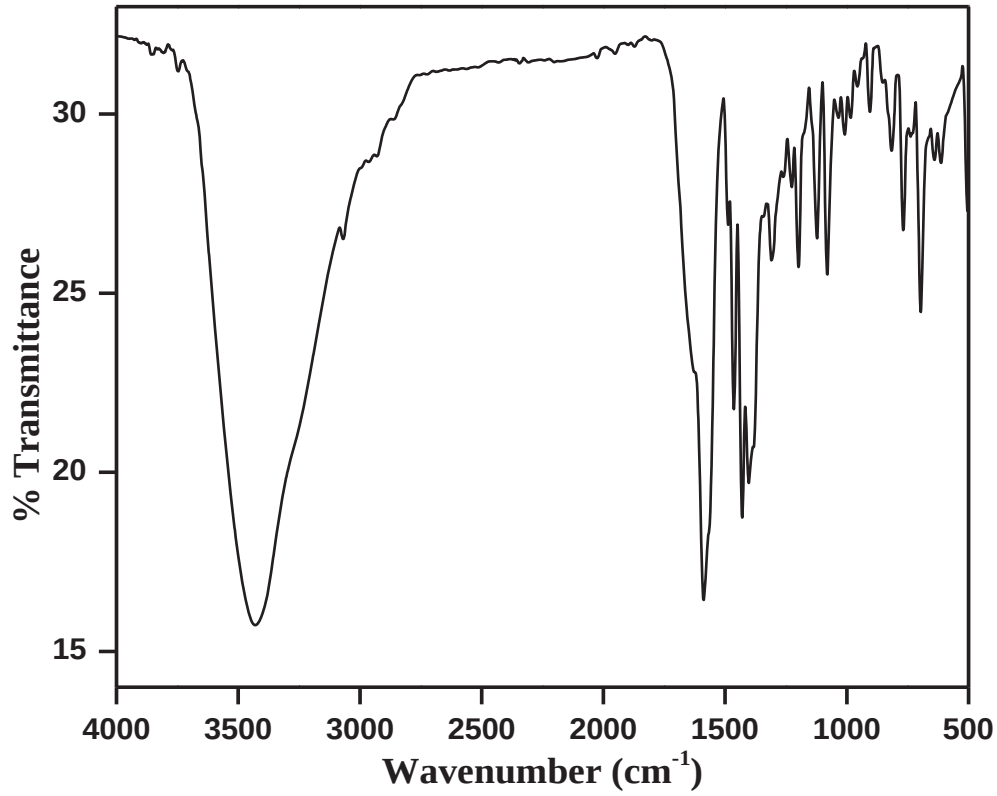

Figure S3. IR spectrum of ligand (L^3).

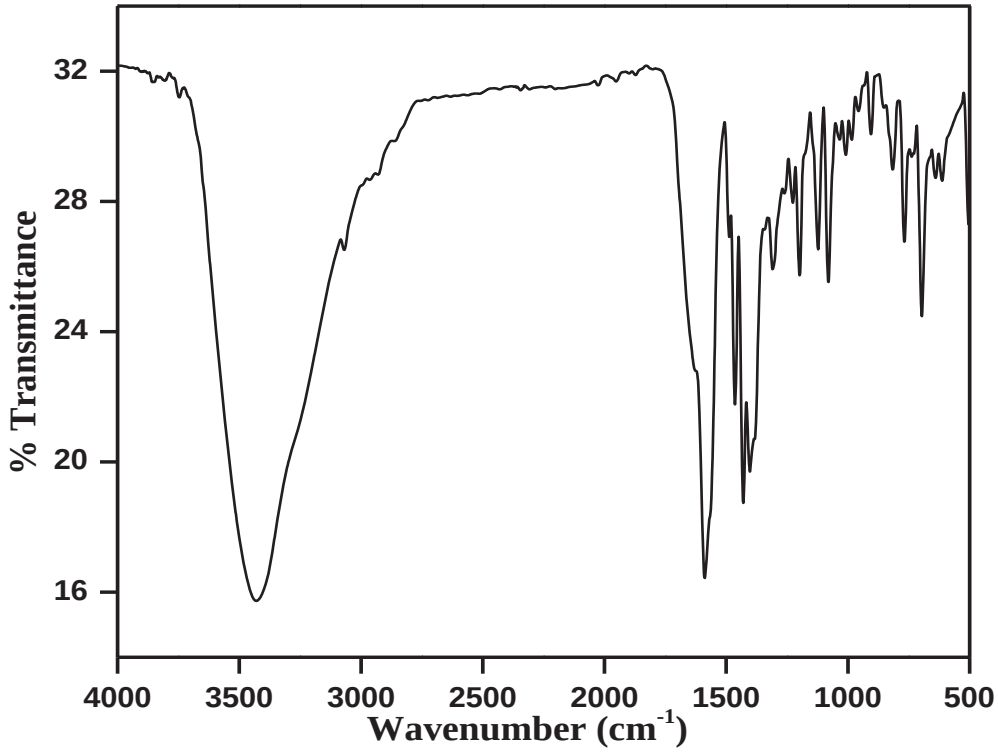

Figure S4. IR spectrum of ligand (L^4).

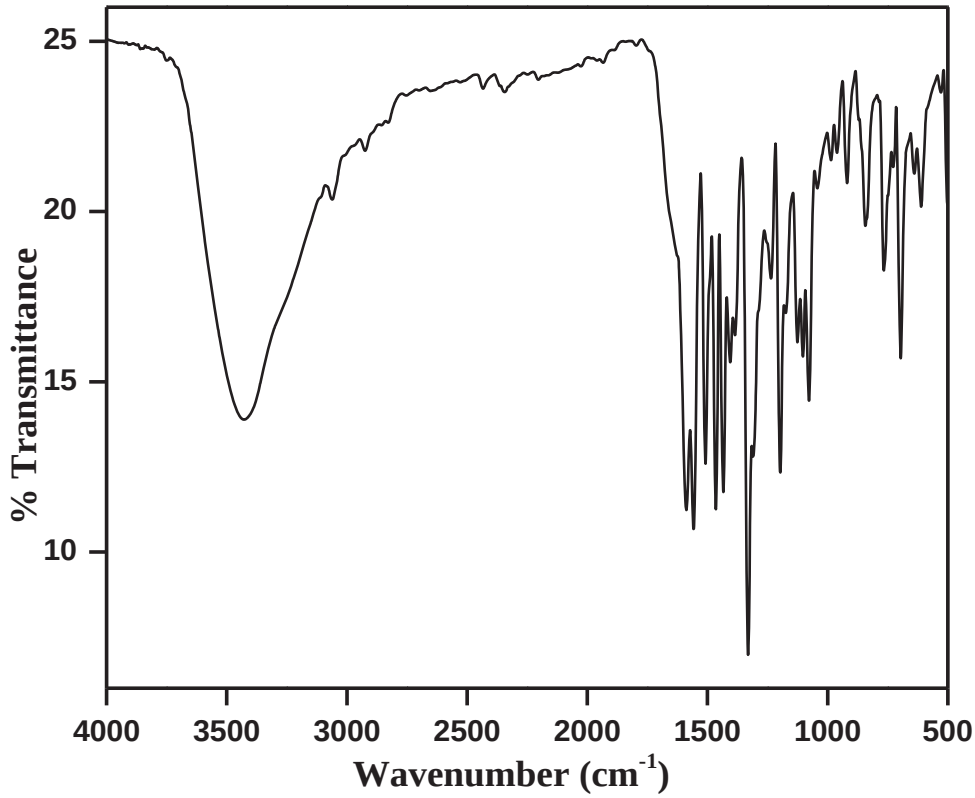

Figure S5. IR spectrum of ligand (L^5).

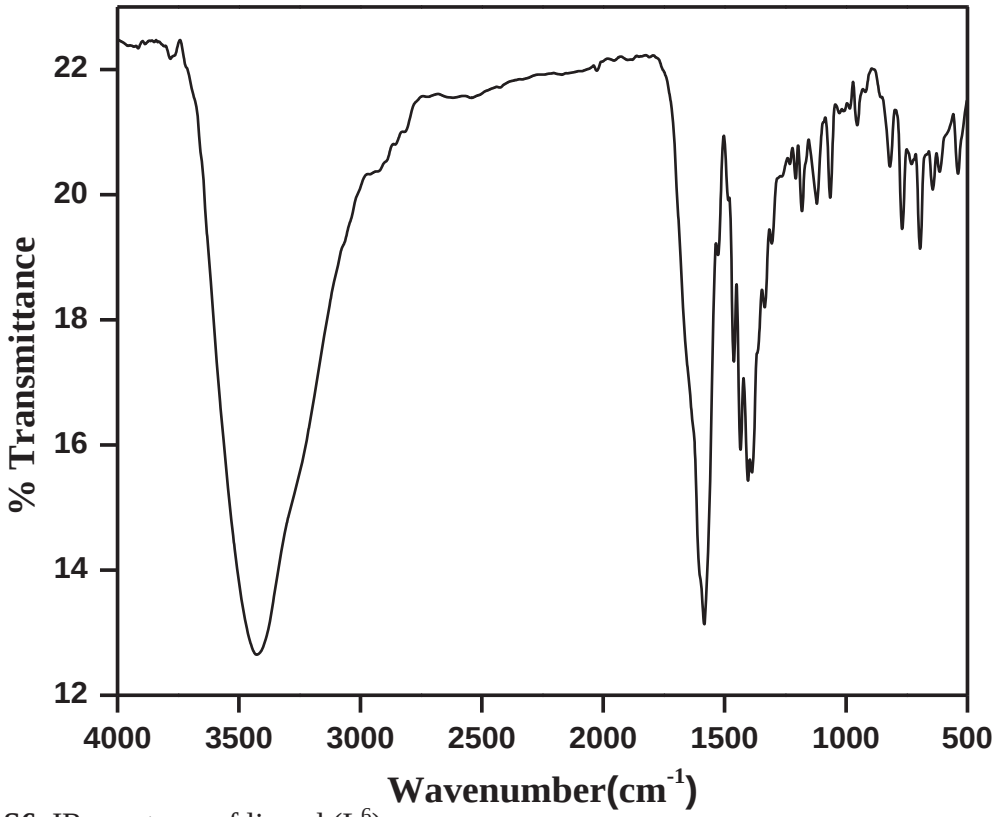

Figure S6. IR spectrum of ligand (L^6).

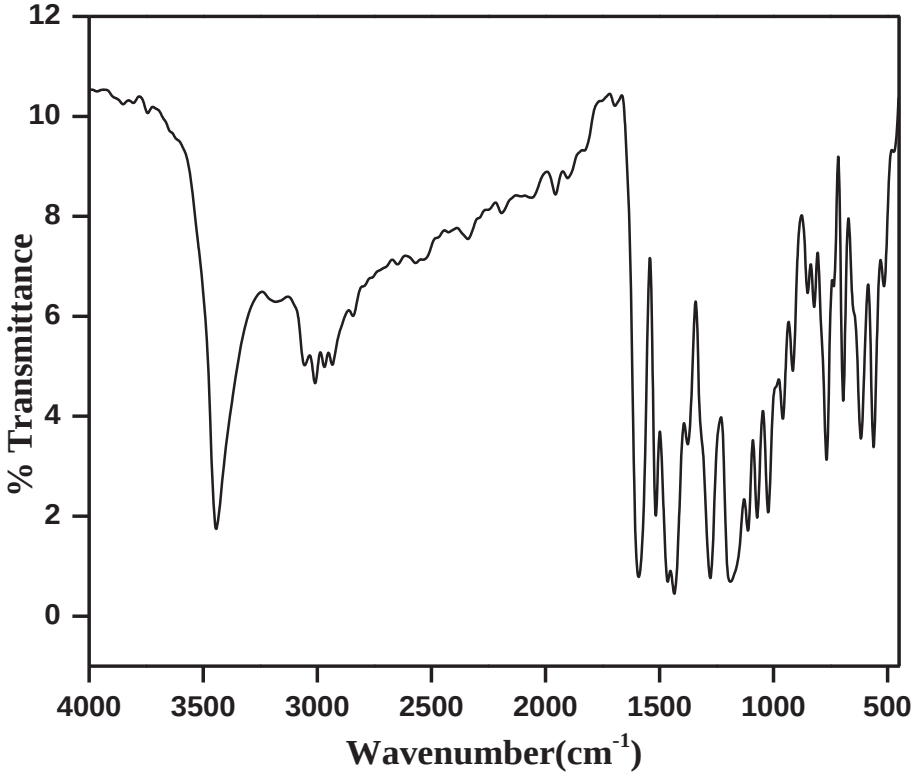

Figure S7. IR spectrum of ligand (L^7).

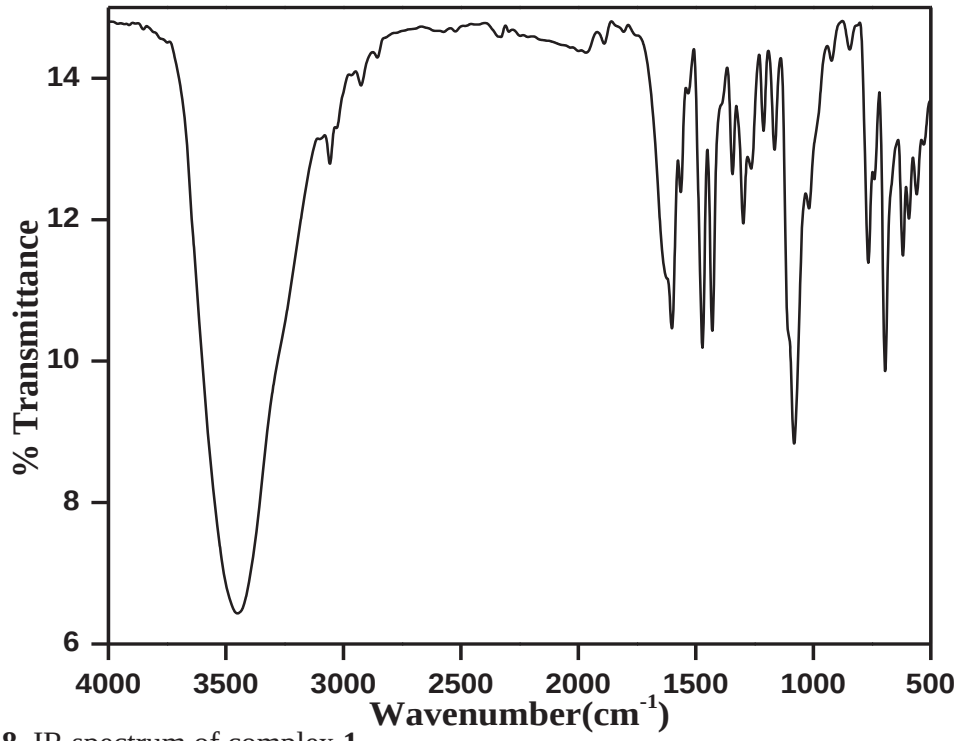

Figure S8. IR spectrum of complex **1**.

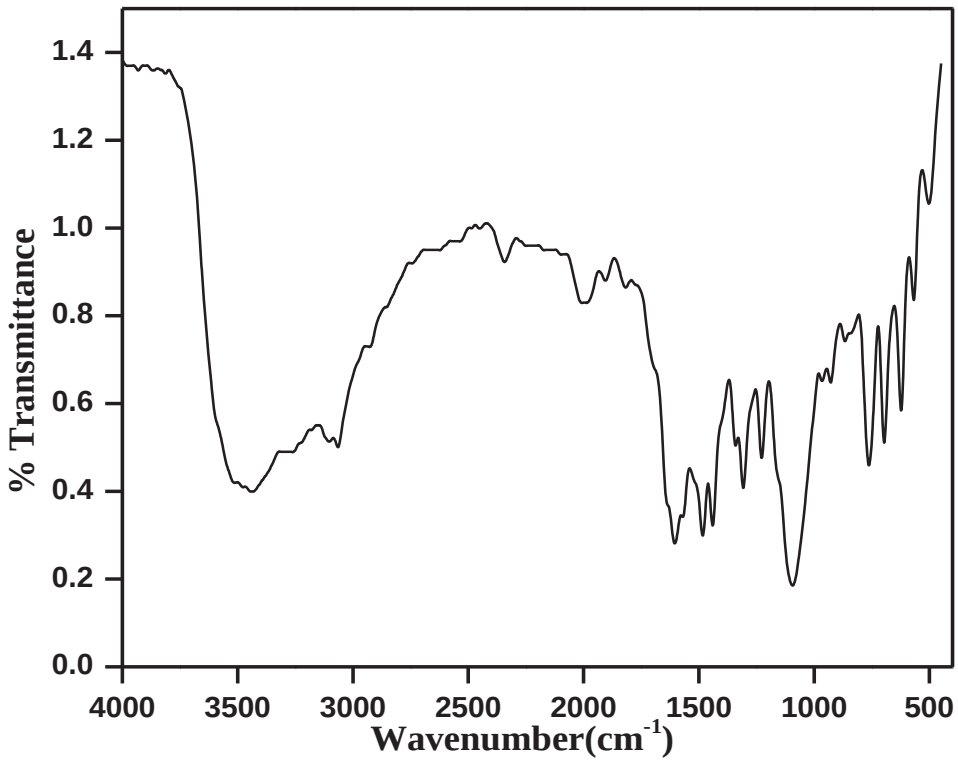

Figure S9. IR spectrum of complex **2**.

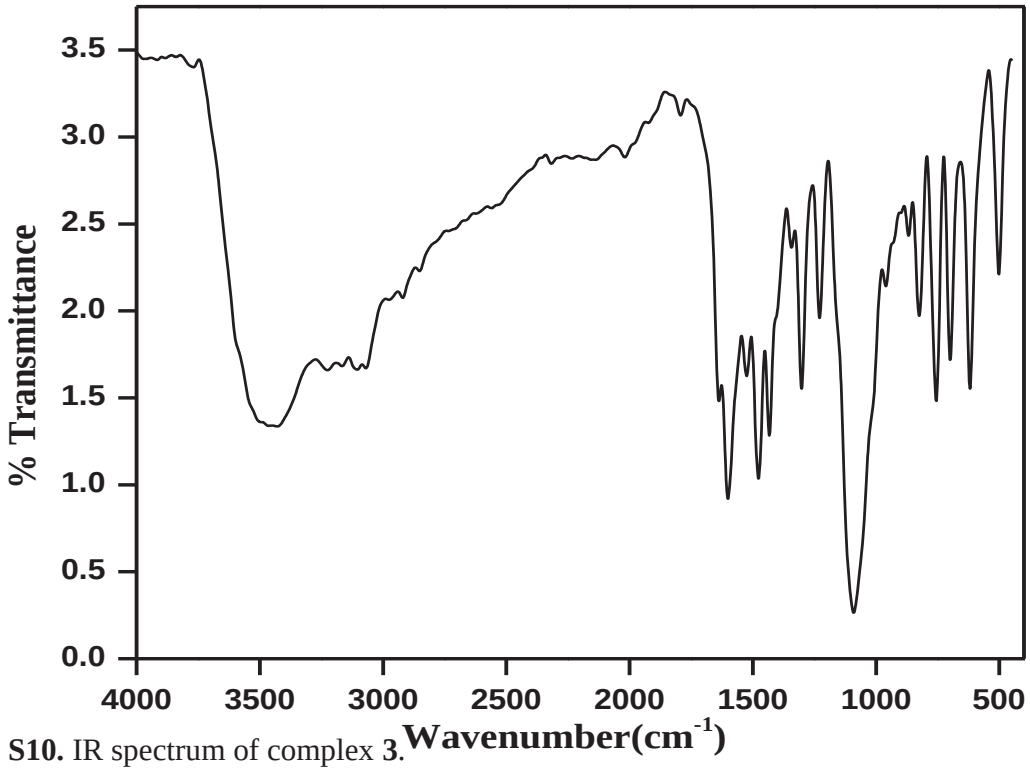

Figure S10. IR spectrum of complex **3**.

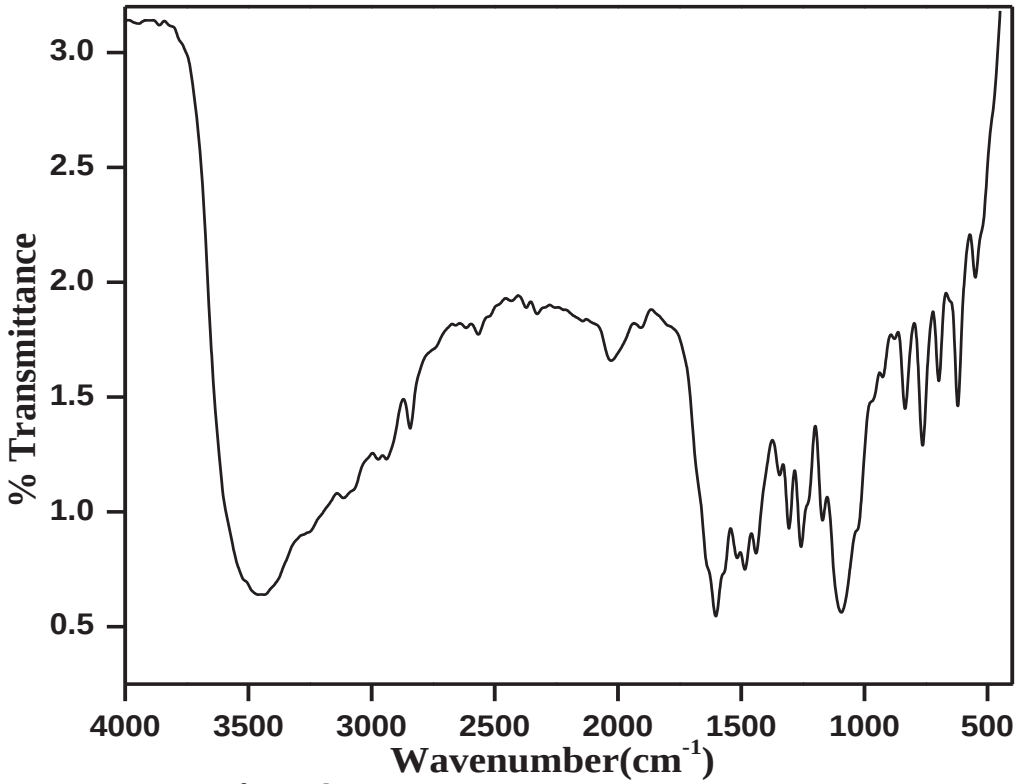

Figure S11. IR spectrum of complex **4**.

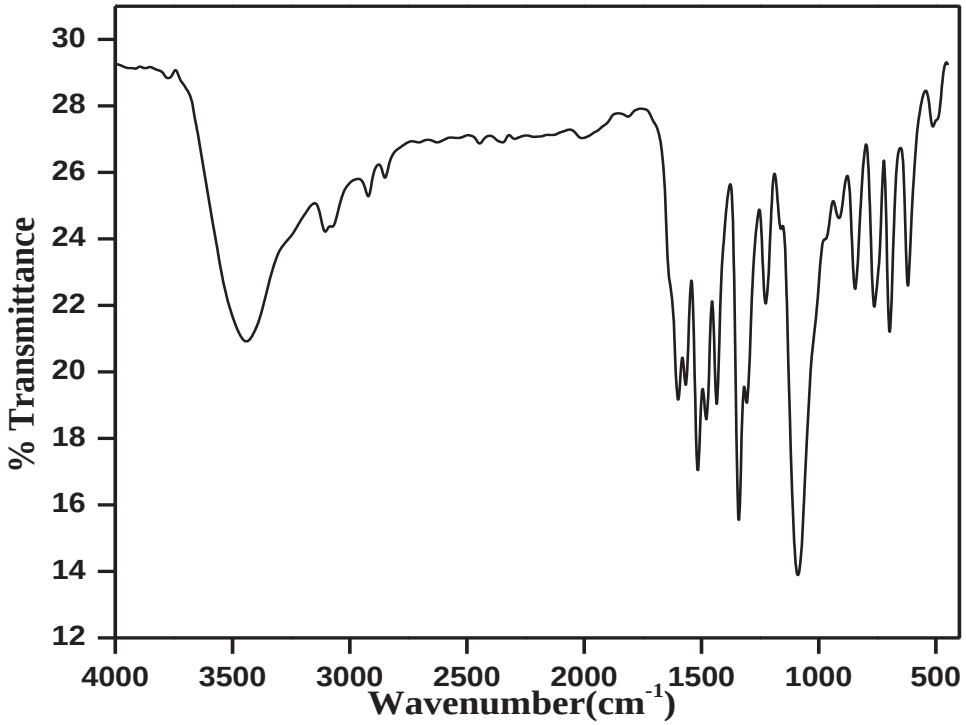

Figure S12. IR spectrum of complex **5**.

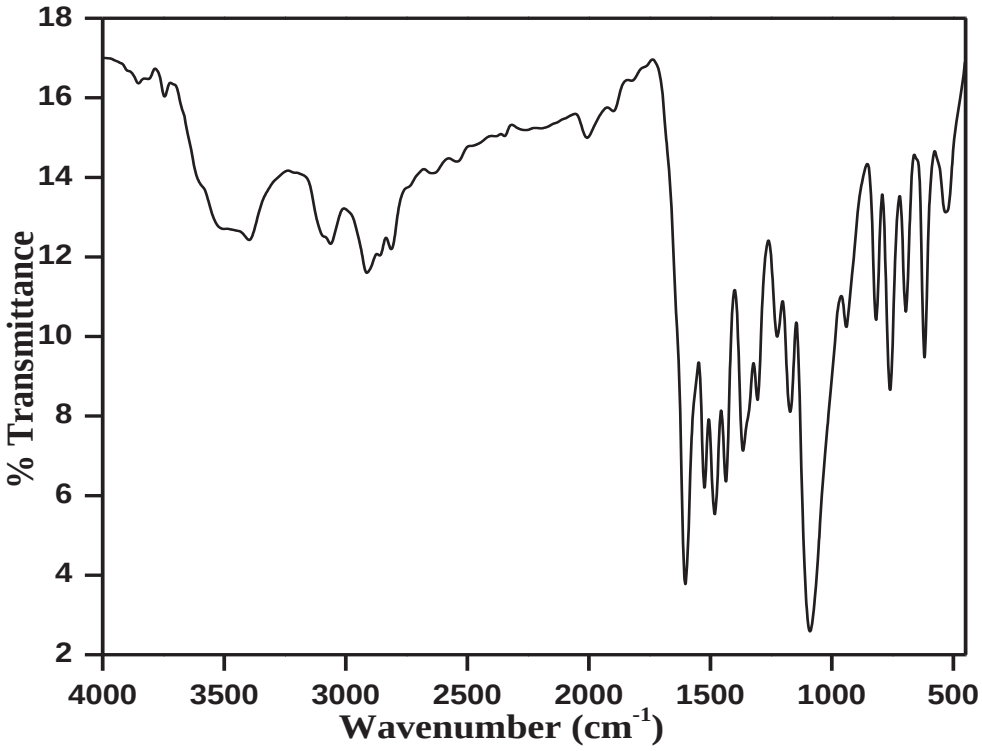

Figure S13. IR spectrum of complex **6**.

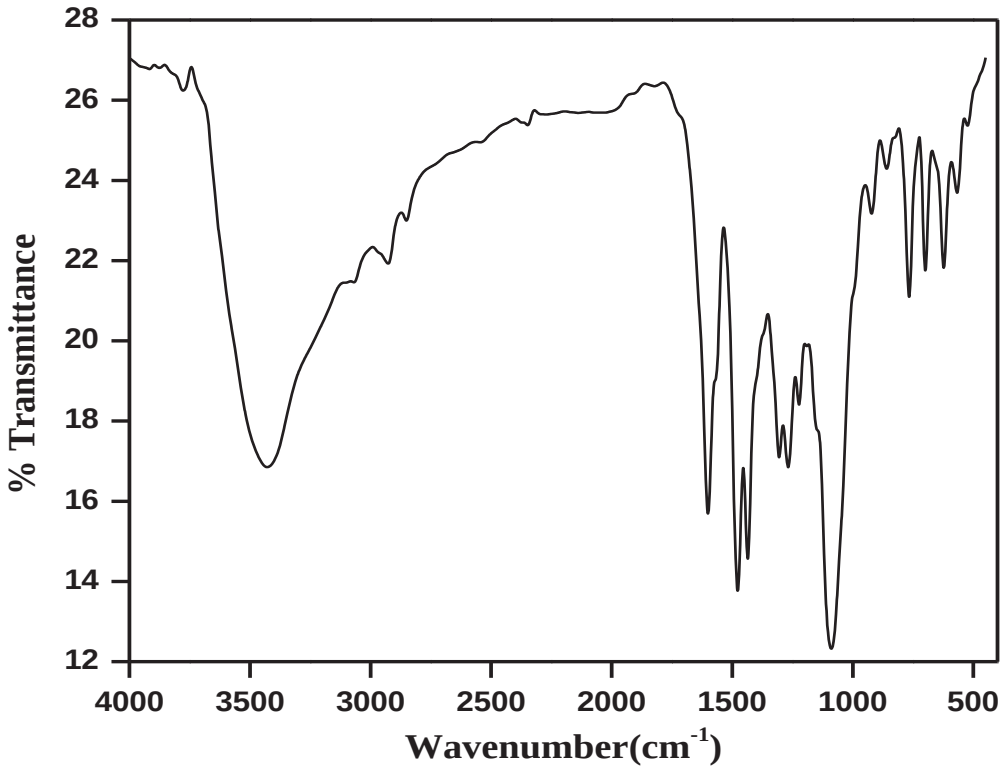

Figure S14. IR spectrum of complex **7**.

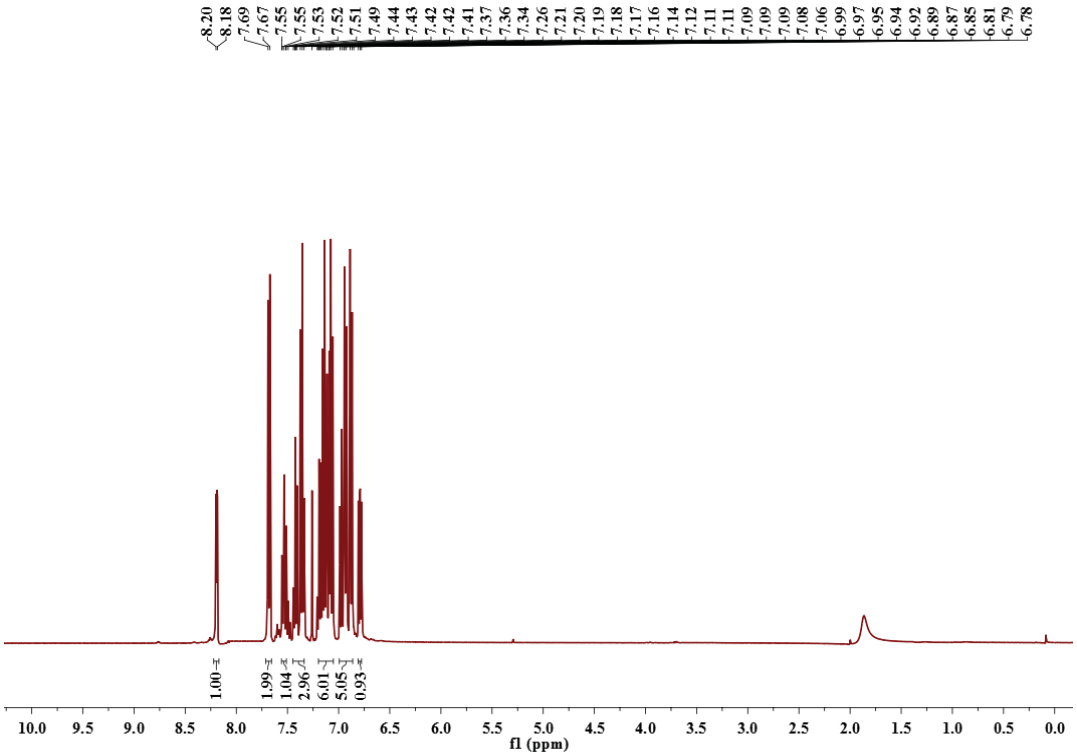

Figure S15. ^{1}H NMR spectrum of ligand (L^{1}) in $CDCl_3$ solvent.

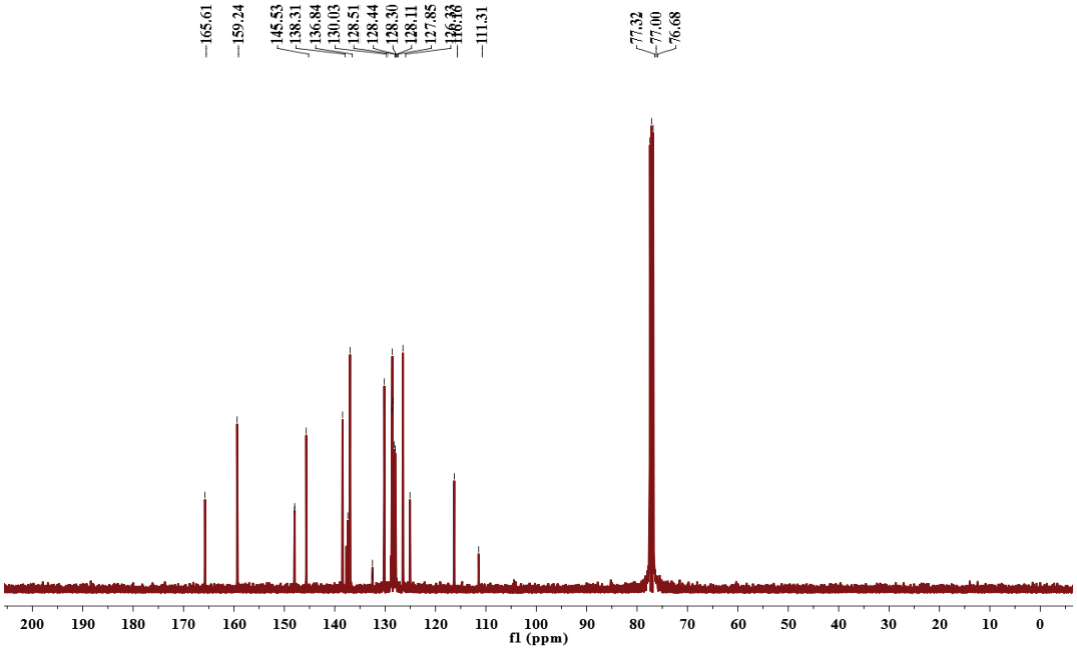

Figure S16. ^{13}C NMR spectrum of ligand (L^{1}) in $CDCl_3$ solvent.

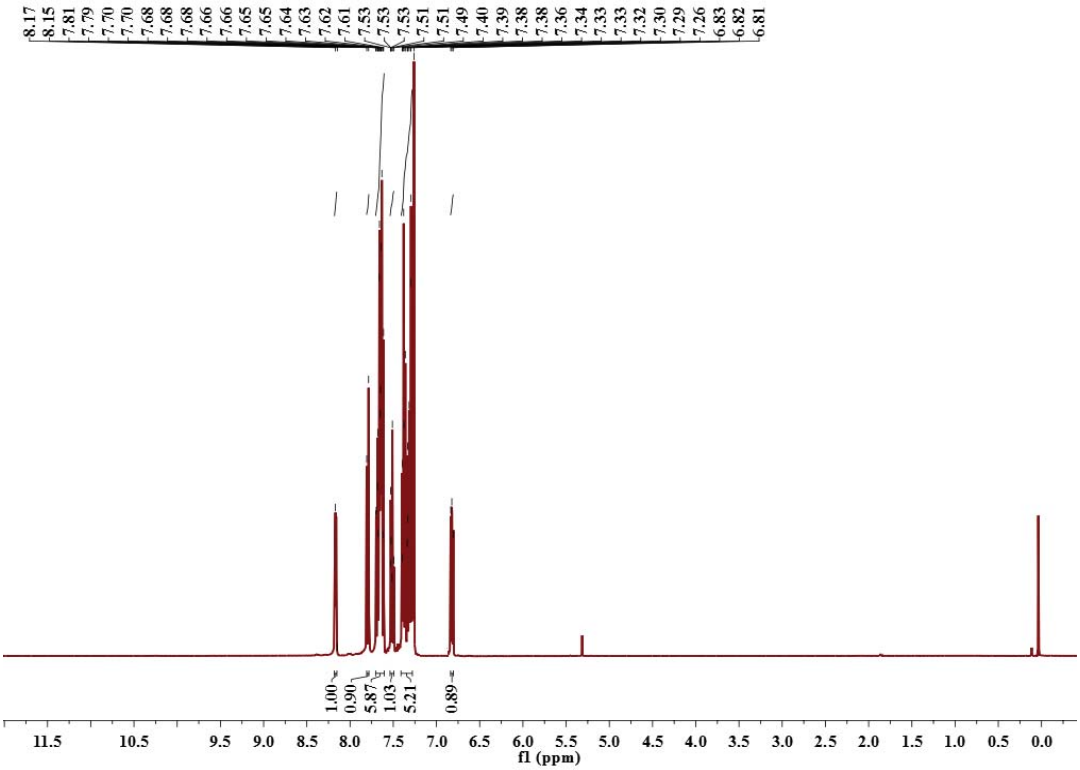

Figure S17. ^{1}H NMR spectrum of ligand (L^2) in $CDCl_3$ solvent.

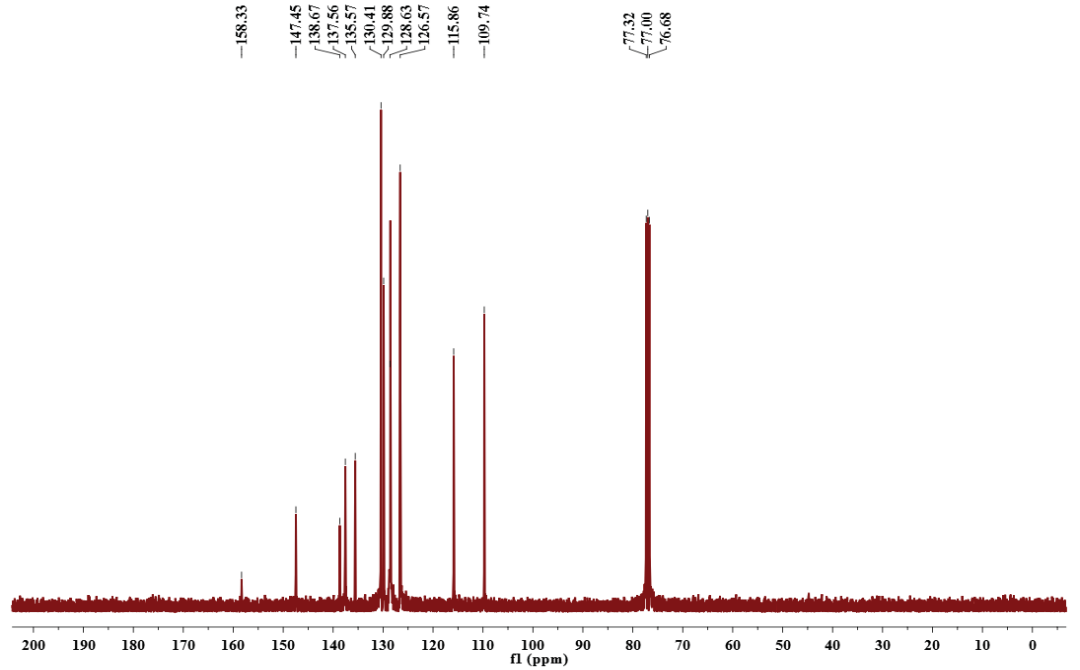

Figure S18. ^{13}C NMR spectrum of ligand (L^2) in $CDCl_3$ solvent.

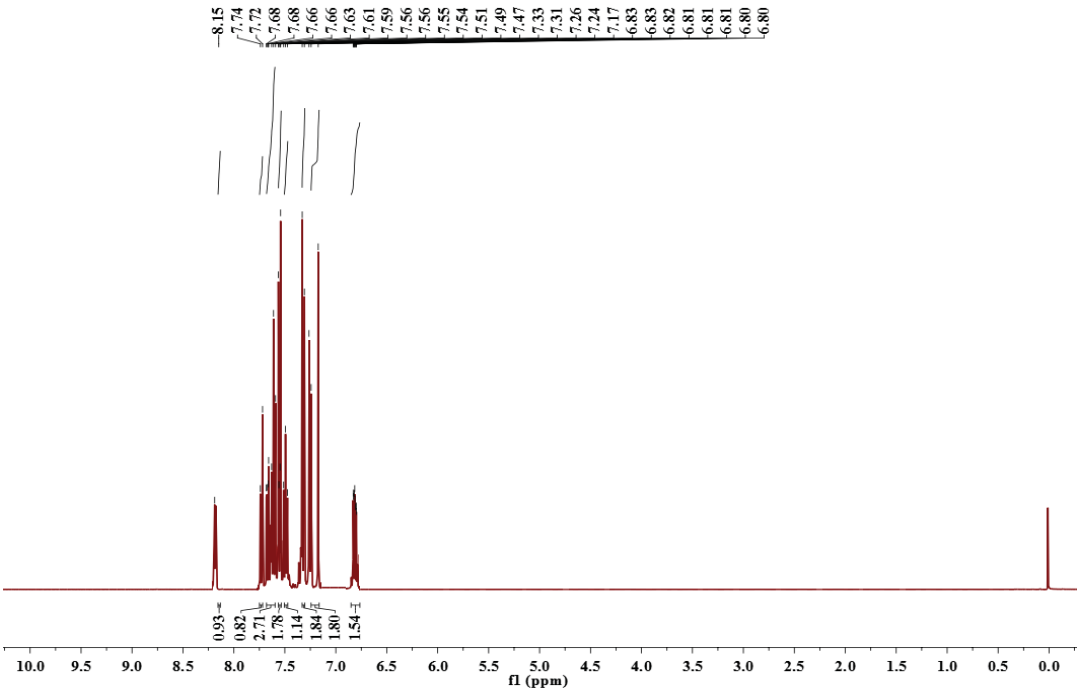

Figure S19. ^{1}H NMR spectrum of ligand (L^3) in $CDCl_3$ solvent.

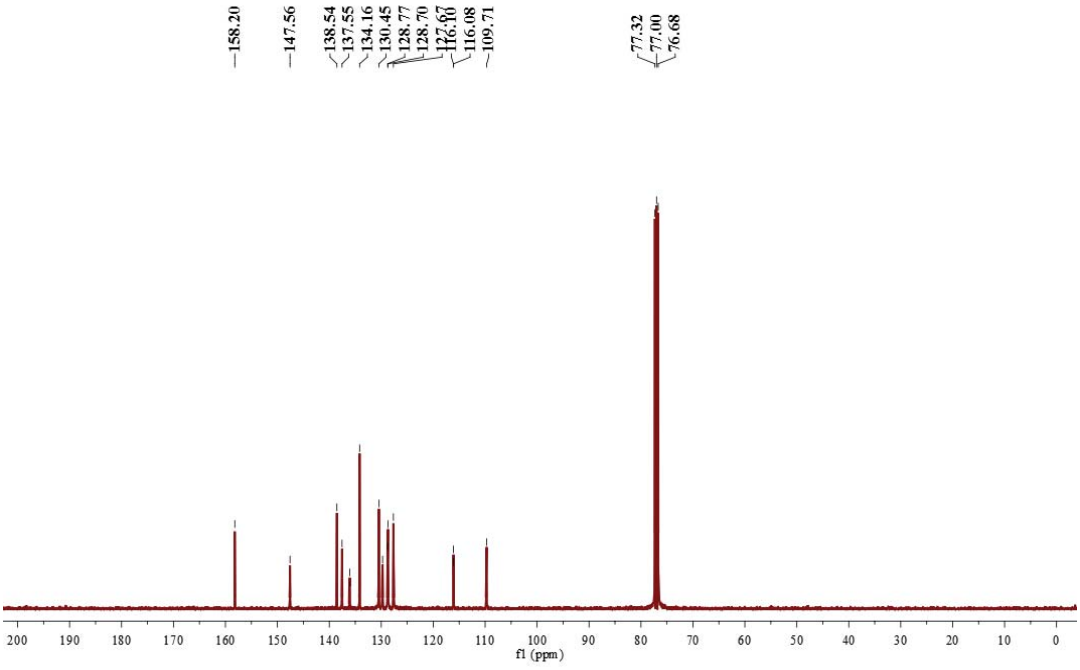

Figure S20. ^{13}C NMR spectrum of ligand (L^3) in $CDCl_3$ solvent.

.

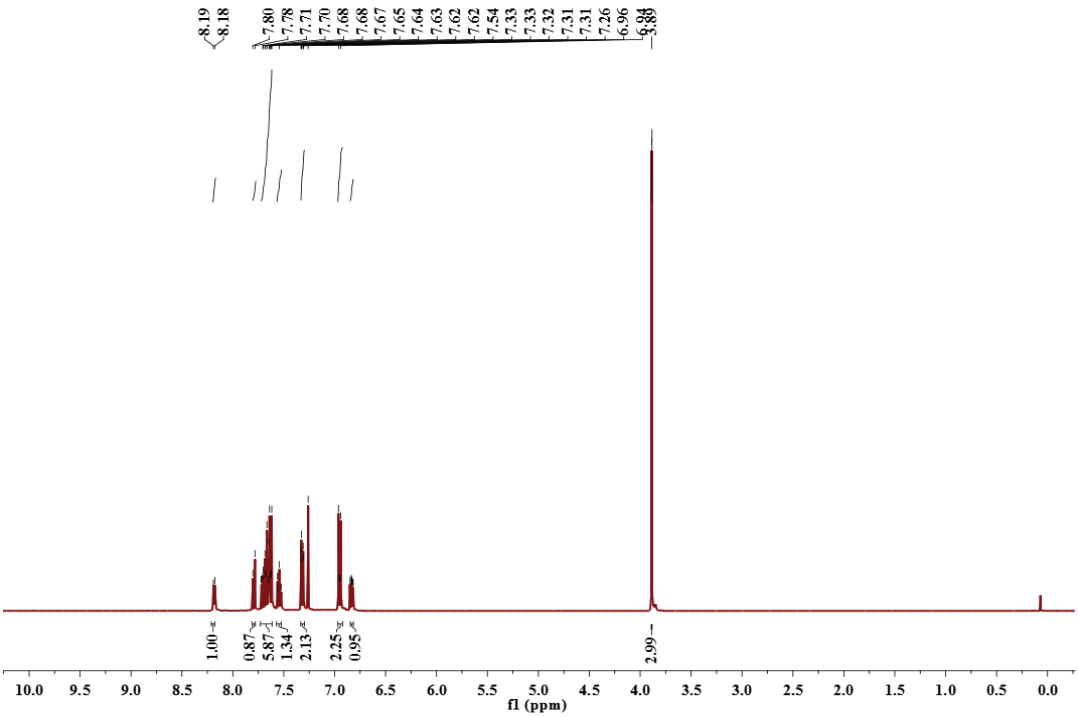

Figure S21. ^{1}H NMR spectrum of ligand (L^4) in $CDCl_3$ solvent.

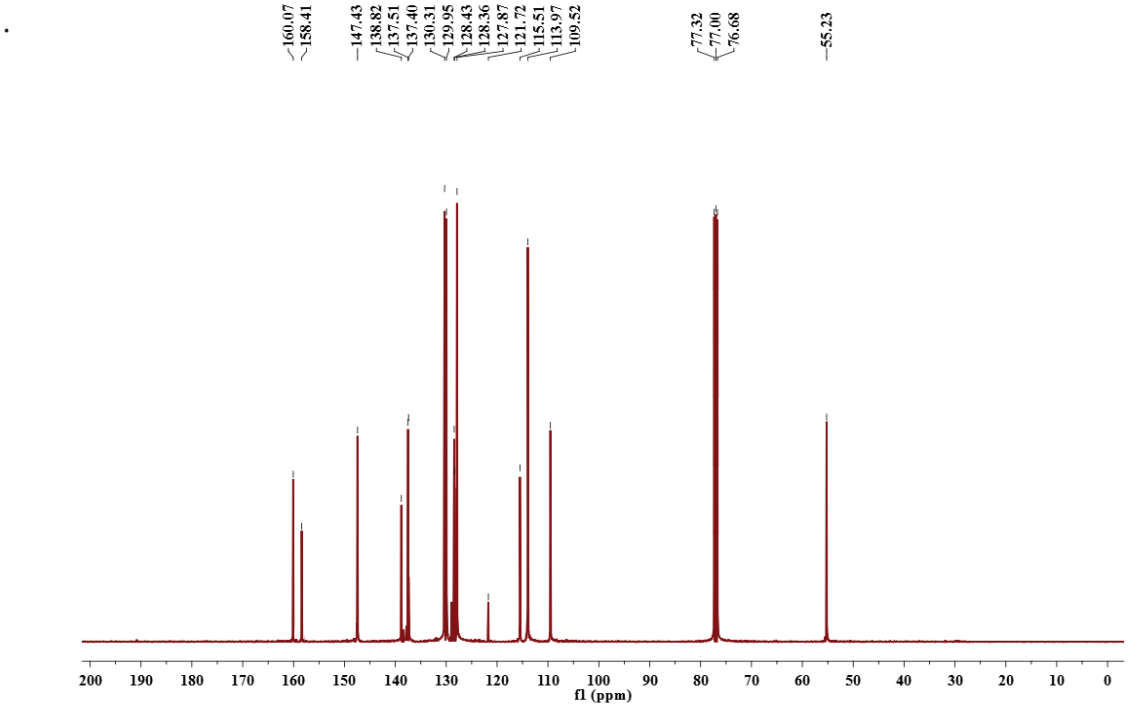

Figure S22. ^{13}C NMR spectrum of ligand (L^4) in $CDCl_3$ solvent.

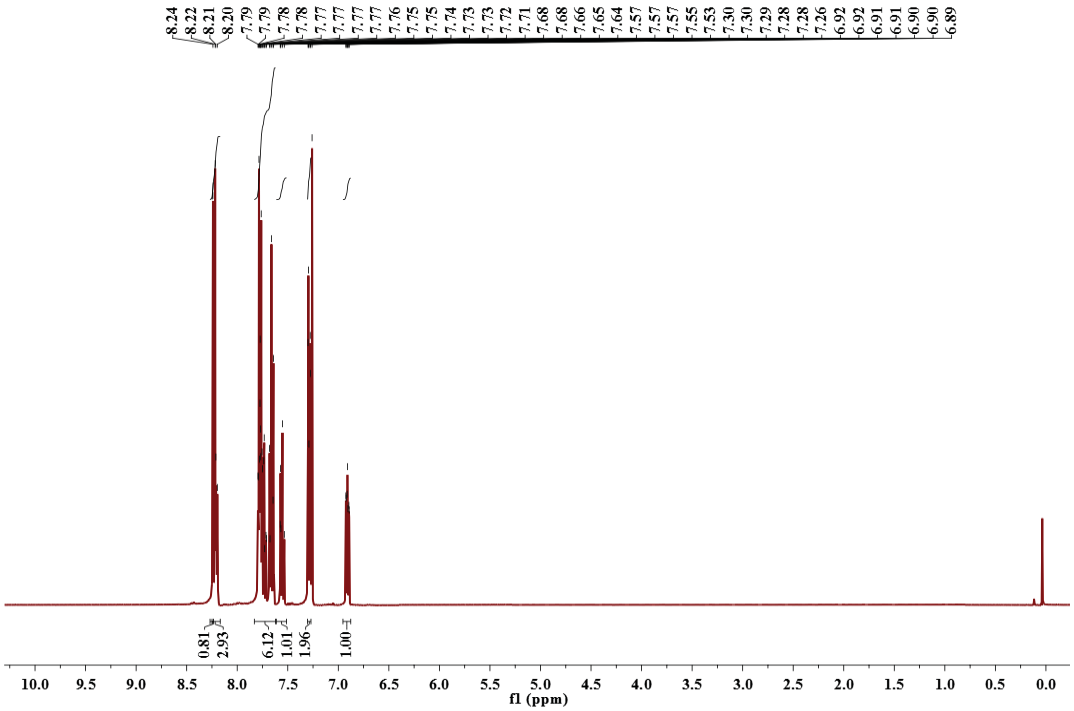

Figure S23. ^{1}H NMR spectrum of ligand (L^5) in $CDCl_3$ solvent.

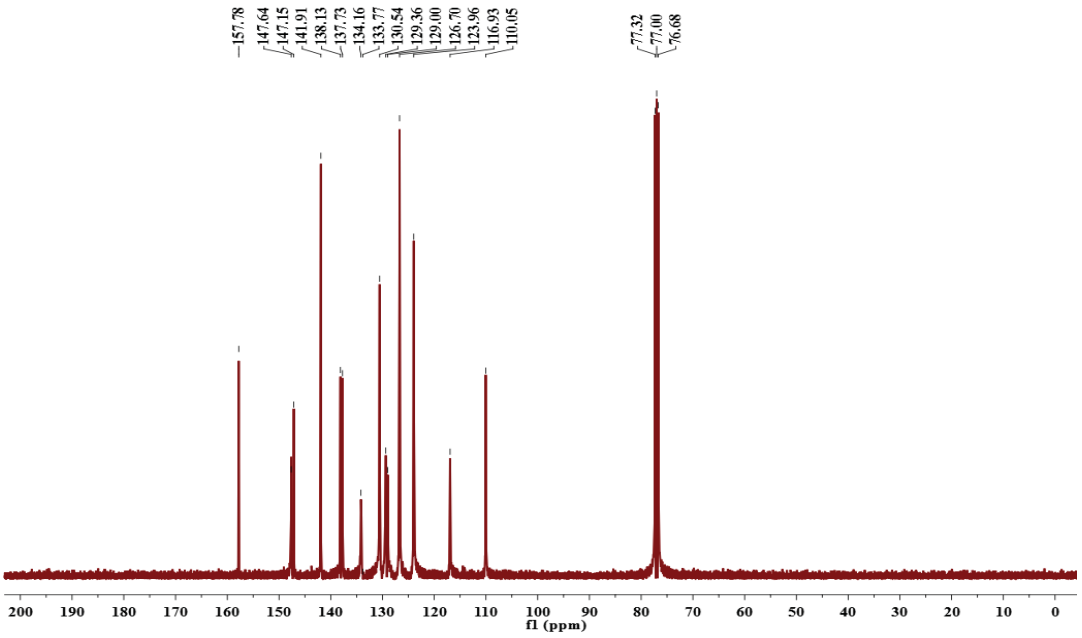

Figure S24. ^{13}C NMR spectrum of ligand (L^5) in $CDCl_3$ solvent.

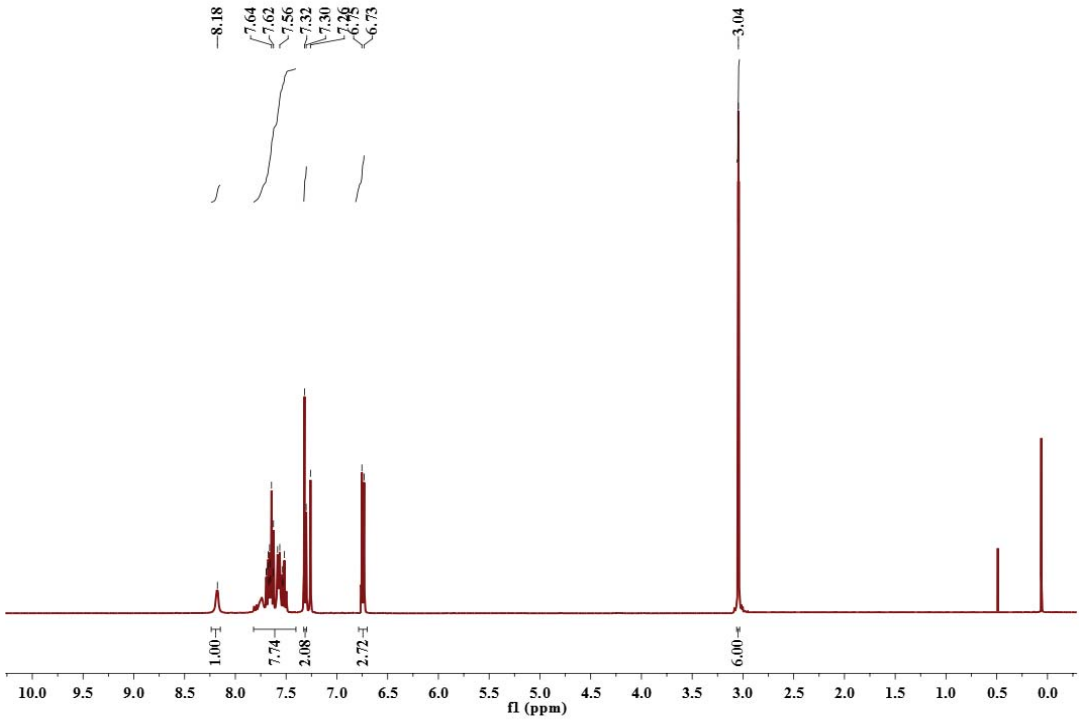

Figure S25. ^{1}H NMR spectrum of ligand (L^{6}) in $CDCl_3$ solvent.

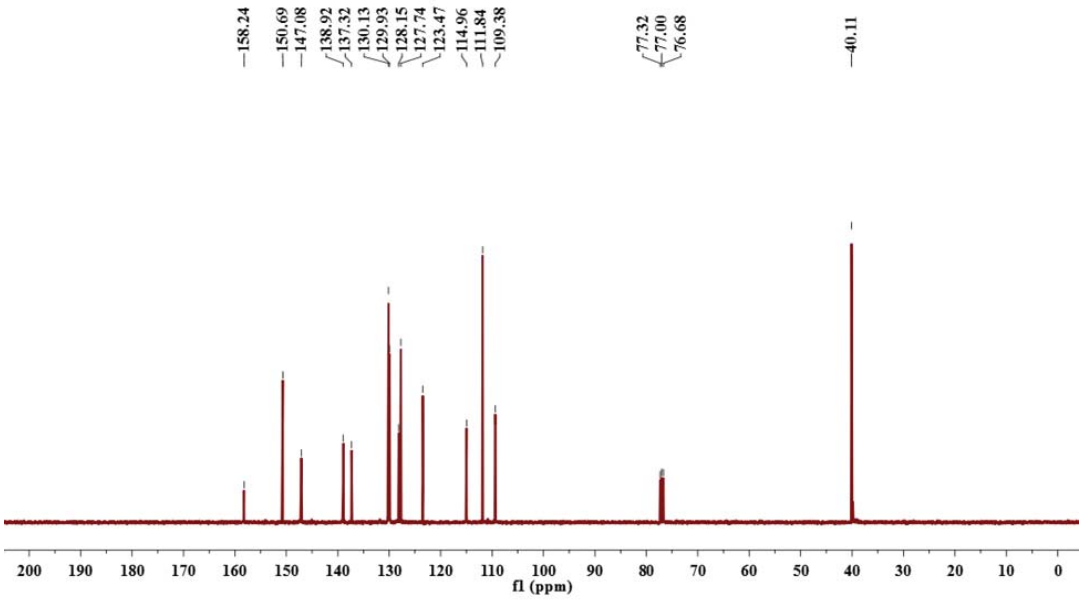

Figure S26. ^{13}C NMR spectrum of ligand (L^{6}) in $CDCl_3$ solvent.

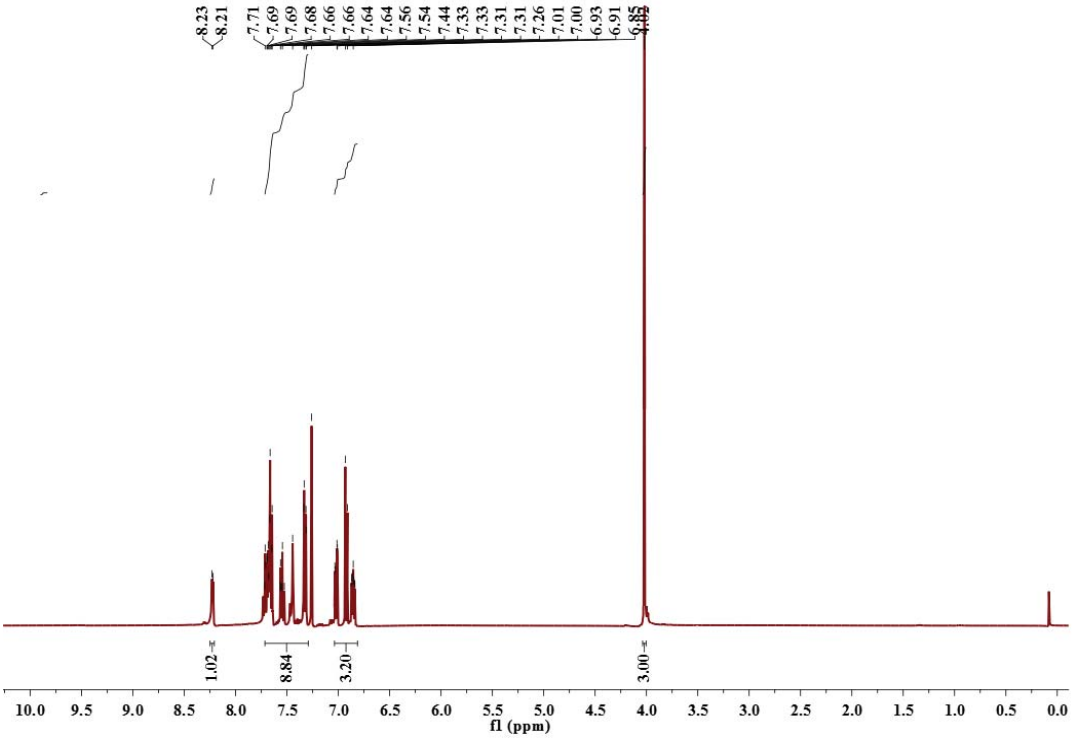

Figure S27. ^{1}H NMR spectrum of ligand (L^{7}) in $CDCl_3$ solvent.

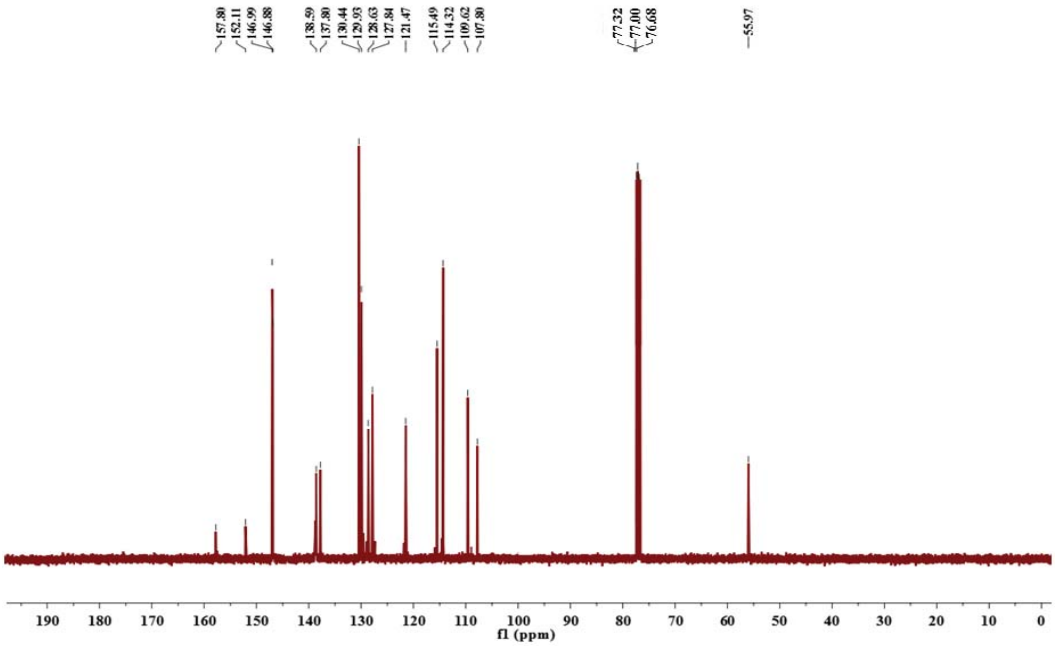

Figure S28. ^{13}C NMR spectrum of ligand (L^{7}) in $CDCl_3$ solvent.

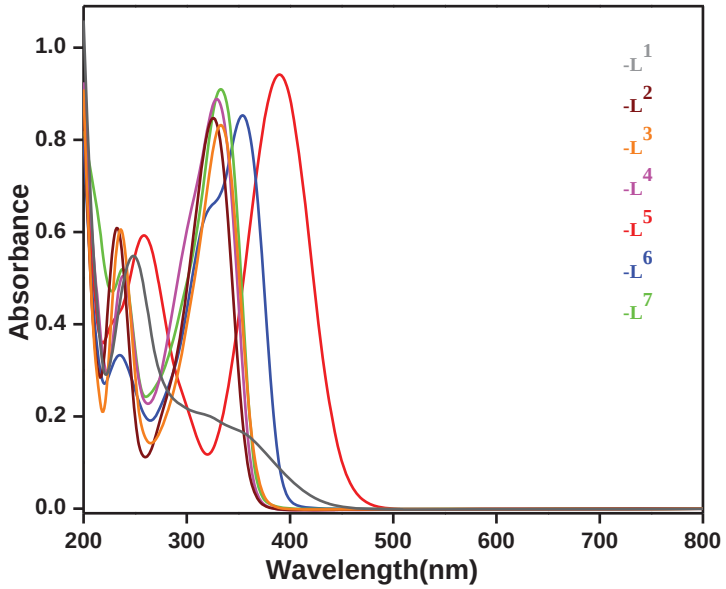

Figure S29. UV-Visible spectra of ligands (L^1-L^7).

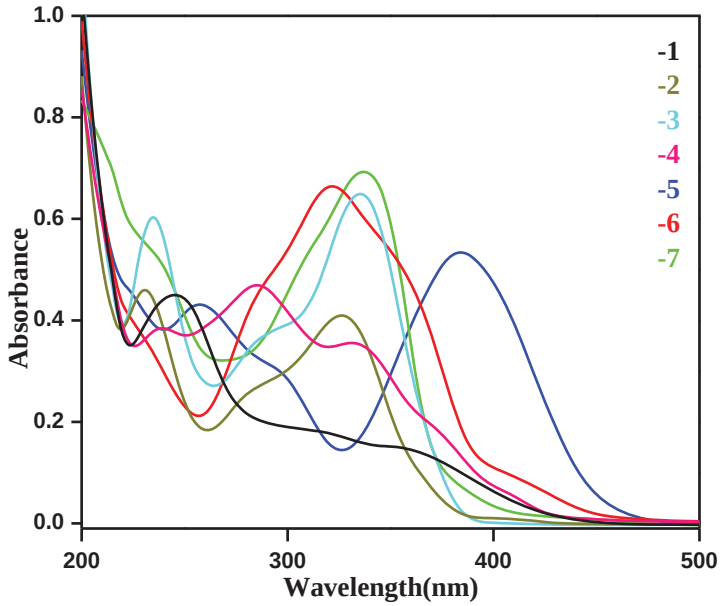

Figure S30. UV-Visible spectra of complexes (**1-7**).

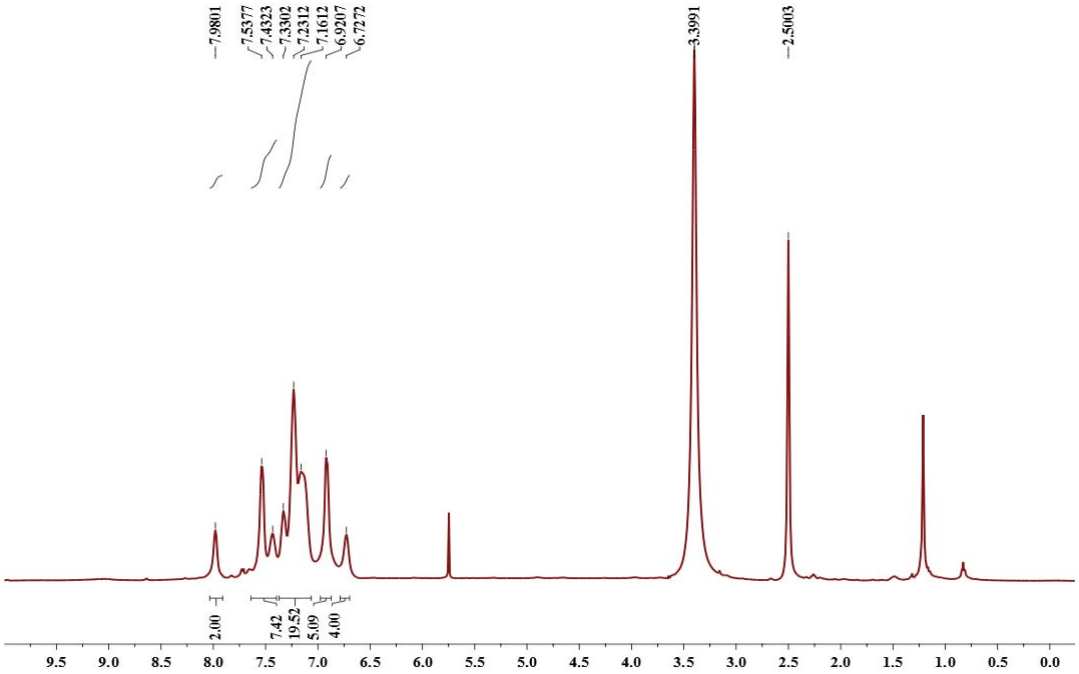

Figure S31. ^{1}H NMR spectrum of complex **1** in dimethyl sulfoxide (d^{6}) solvent.

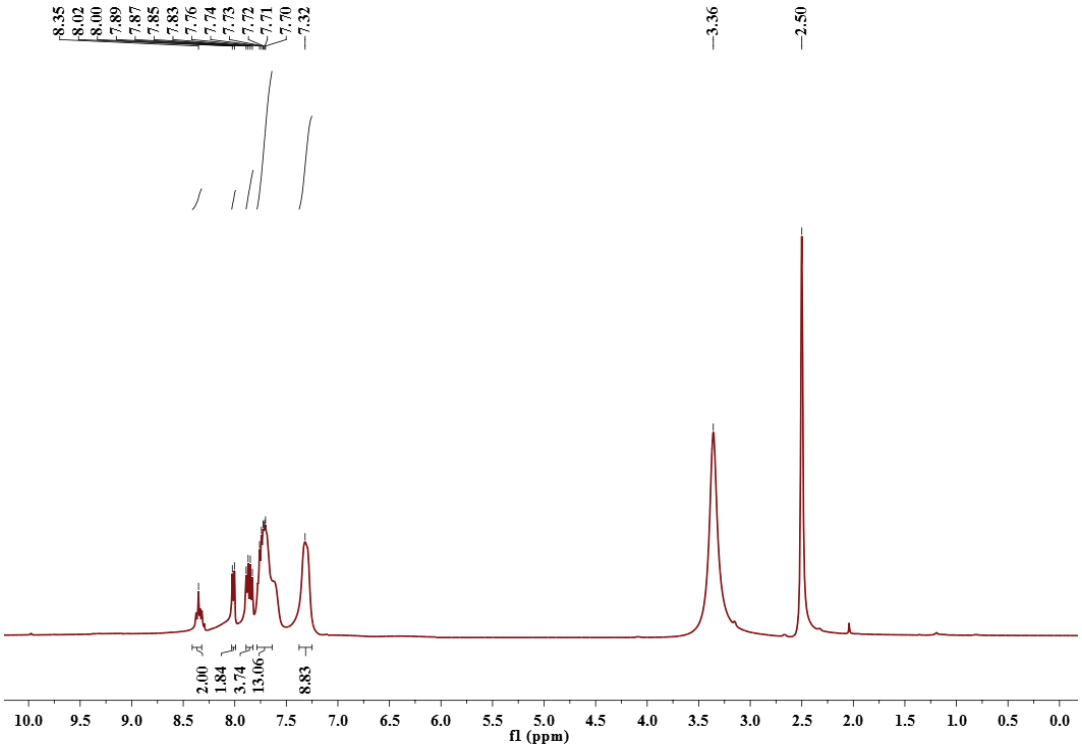

Figure S32. ^{1}H NMR spectrum of complex **2** in dimethyl sulfoxide (d^{6}) solvent.

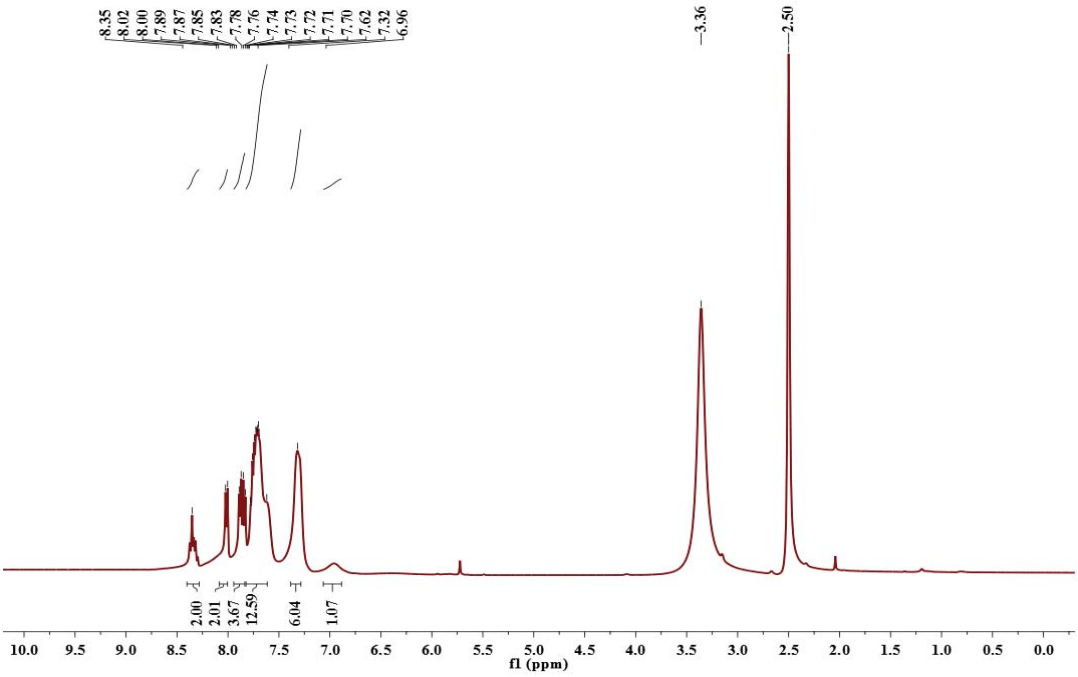

Figure S33. ^{1}H NMR spectrum of complex **3** in dimethyl sulfoxide (d^{6}) solvent.

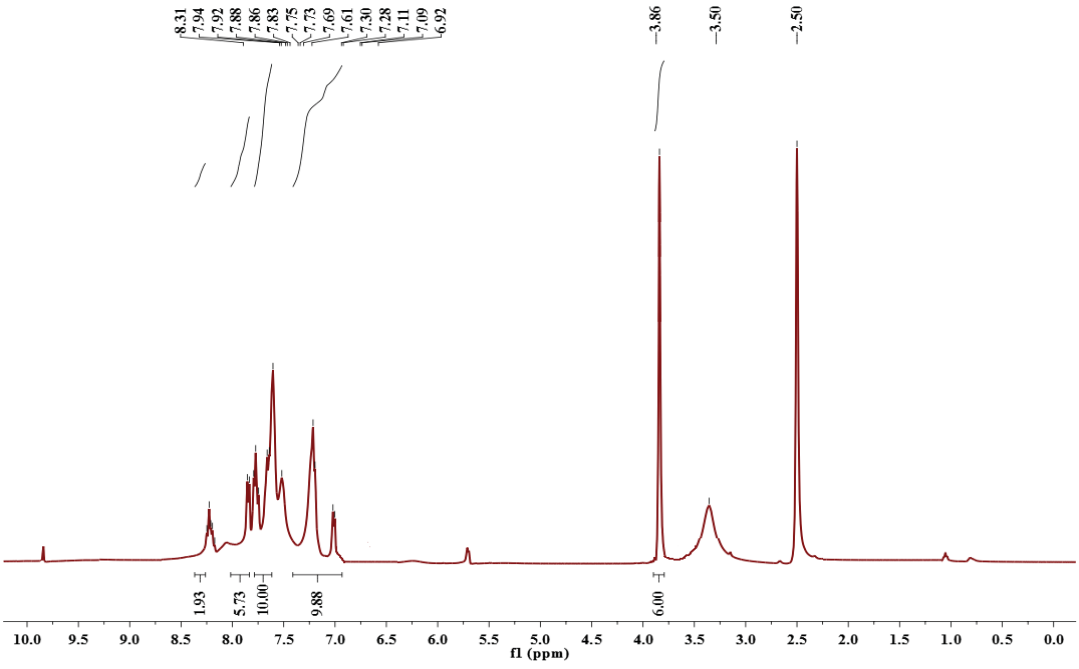

Figure S34. ^{1}H NMR spectrum of complex **4** in dimethyl sulfoxide (d^{6}) solvent.

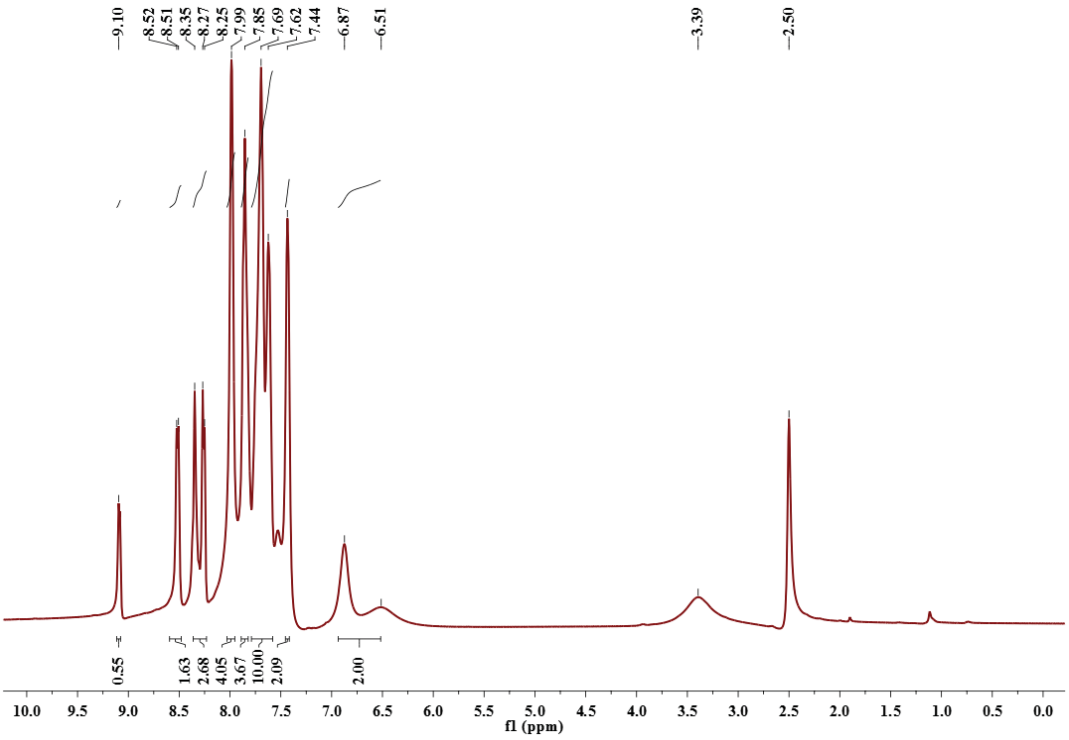

Figure S35. ^{1}H NMR spectrum of complex **5** in dimethyl sulfoxide (d^6) solvent.

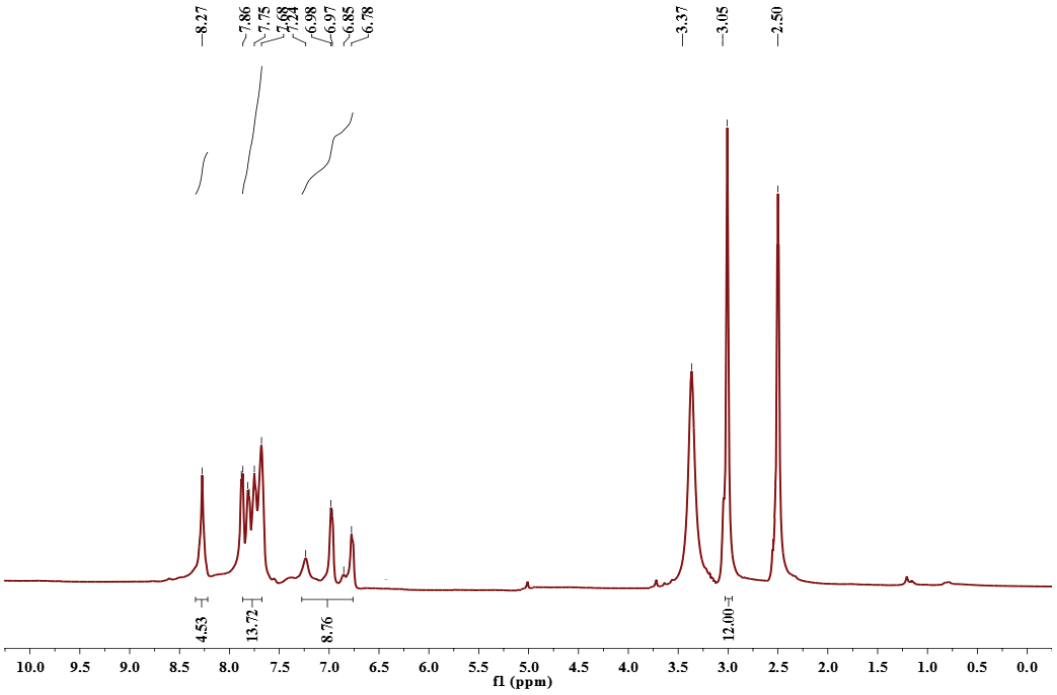

Figure S36. ^{1}H NMR spectrum of complex **6** in dimethyl sulfoxide (d^6) solvent.

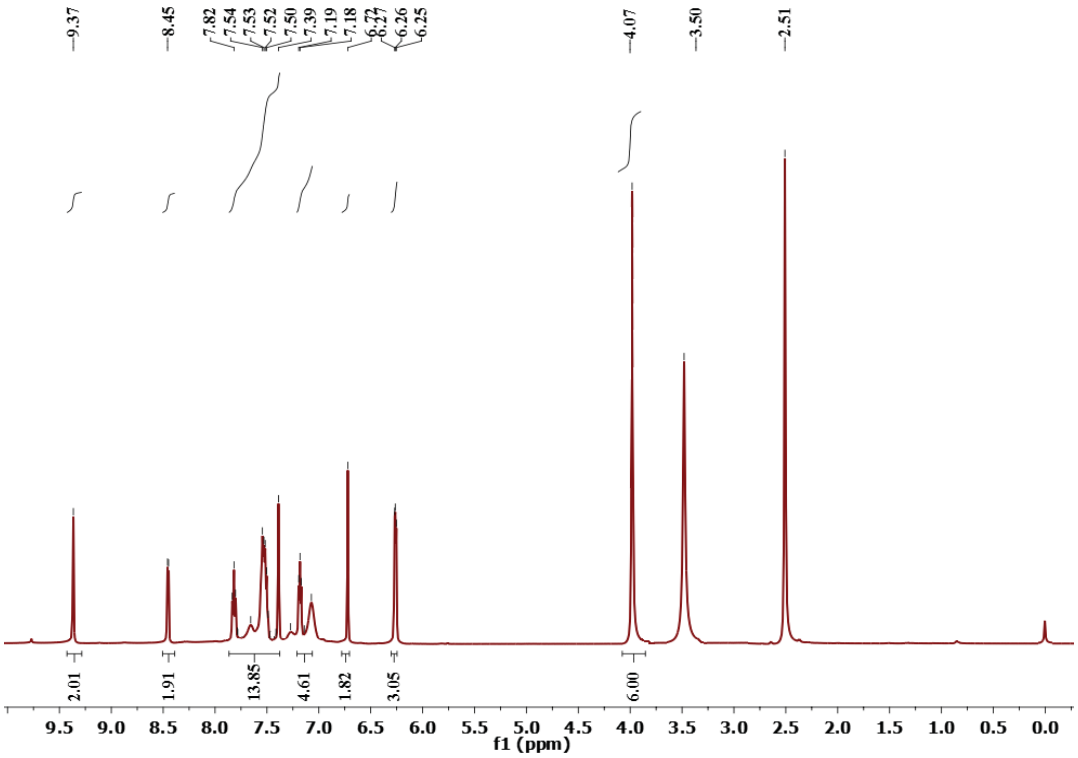

Figure S37. ^{1}H NMR spectrum of complex **7** in dimethyl sulfoxide (d^6) solvent.

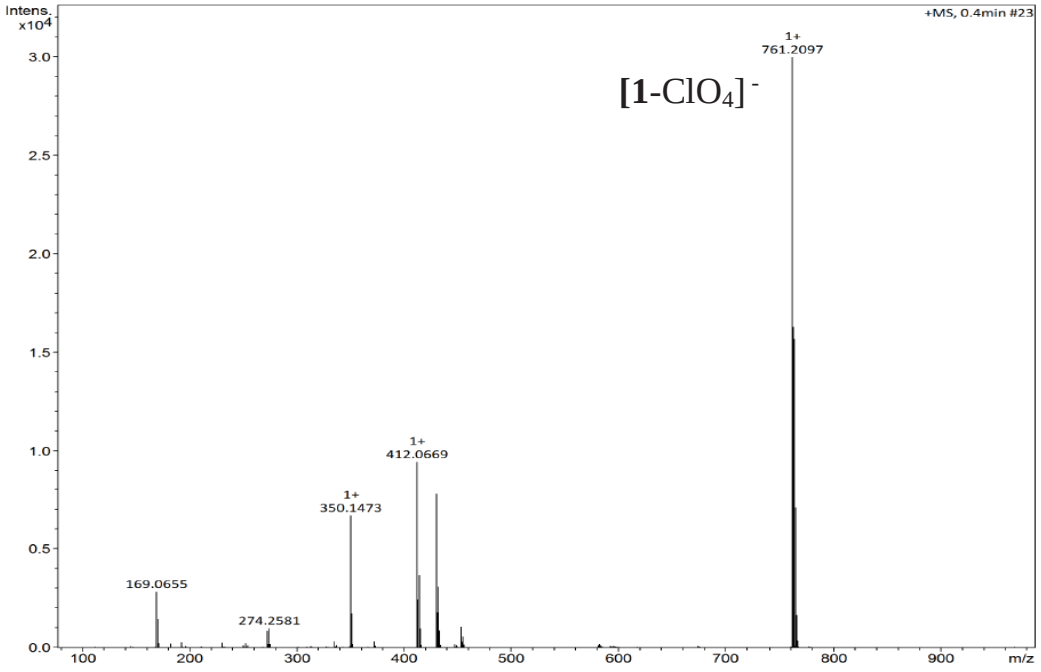

Figure S38. HRMS spectrum of complex **1.**

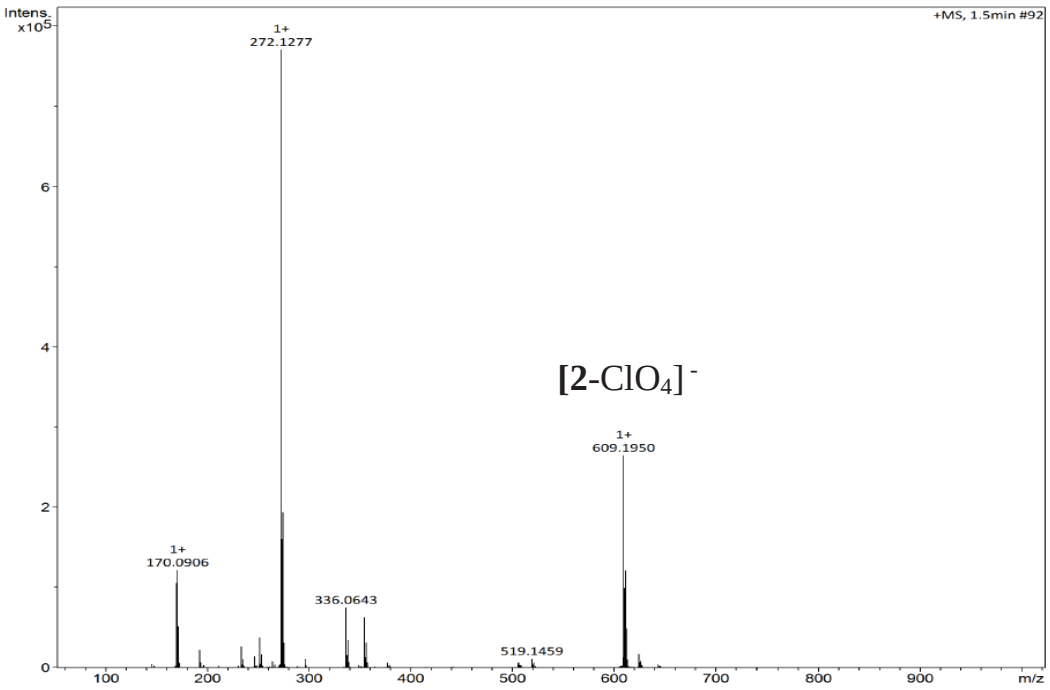

Figure S39. HRMS spectrum of complex **2.**

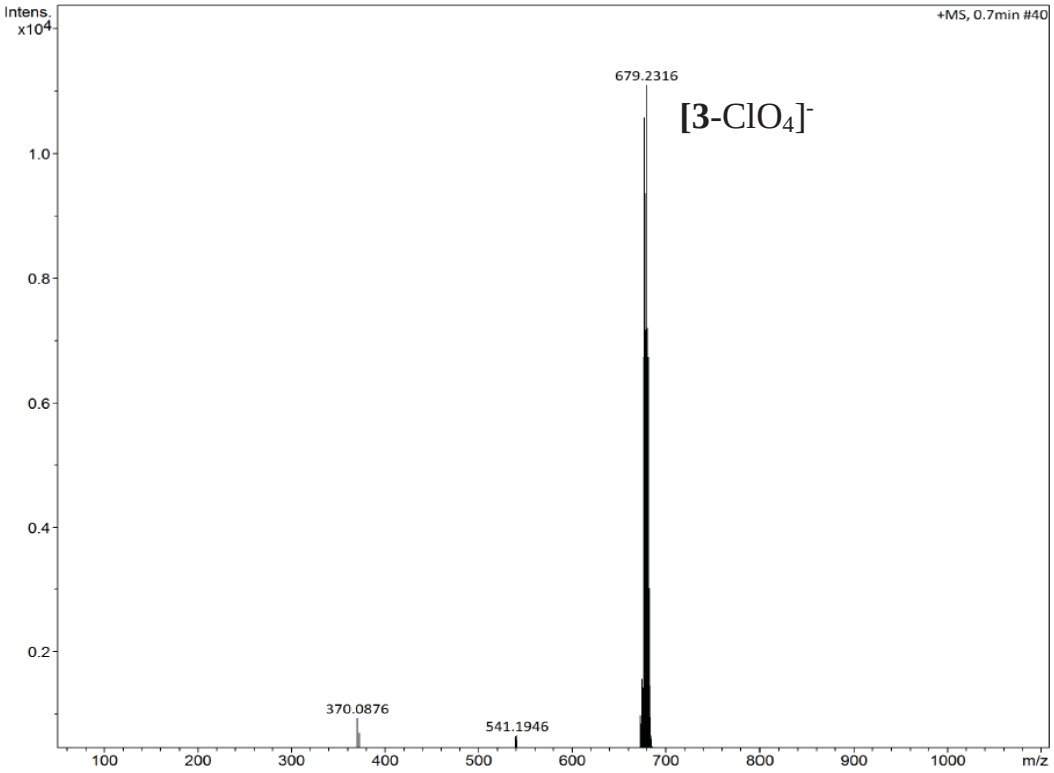

Figure S40. HRMS spectrum of complex **3.**

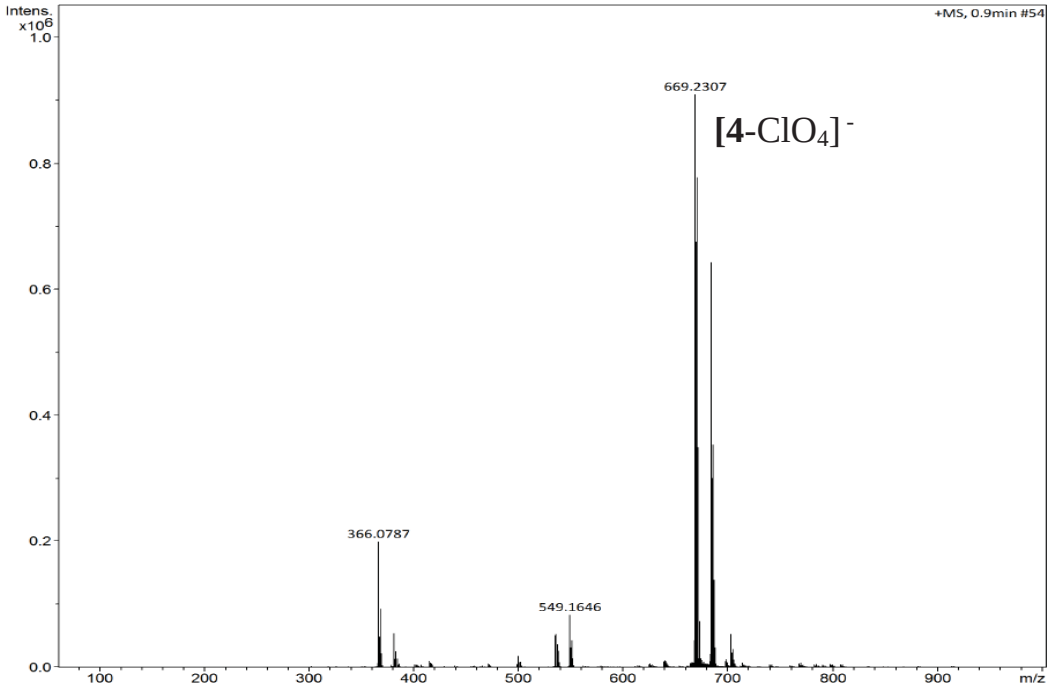

Figure S41. HRMS spectrum of complex **4.**

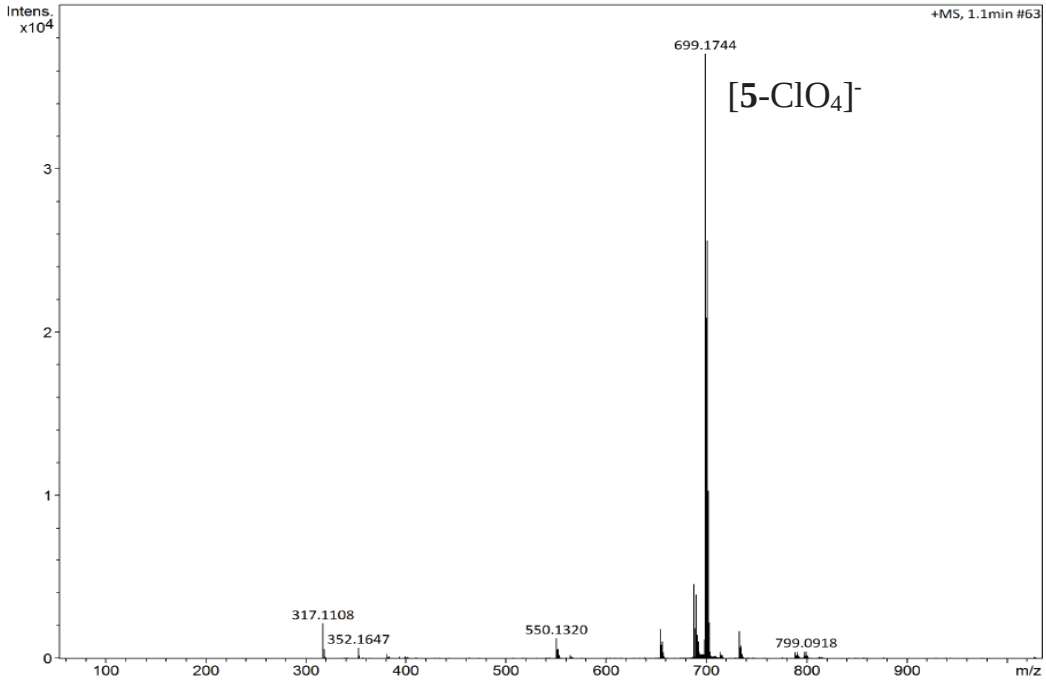

Figure S42. HRMS spectrum of complex **5.**

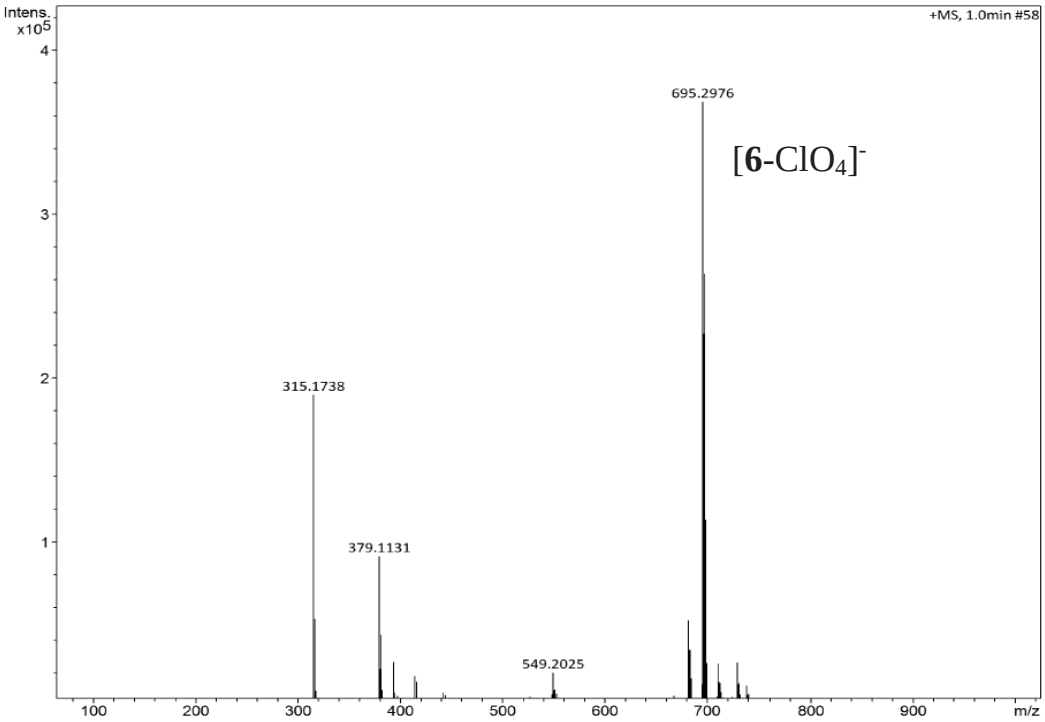

Figure S43. HRMS spectrum of complex **6.**

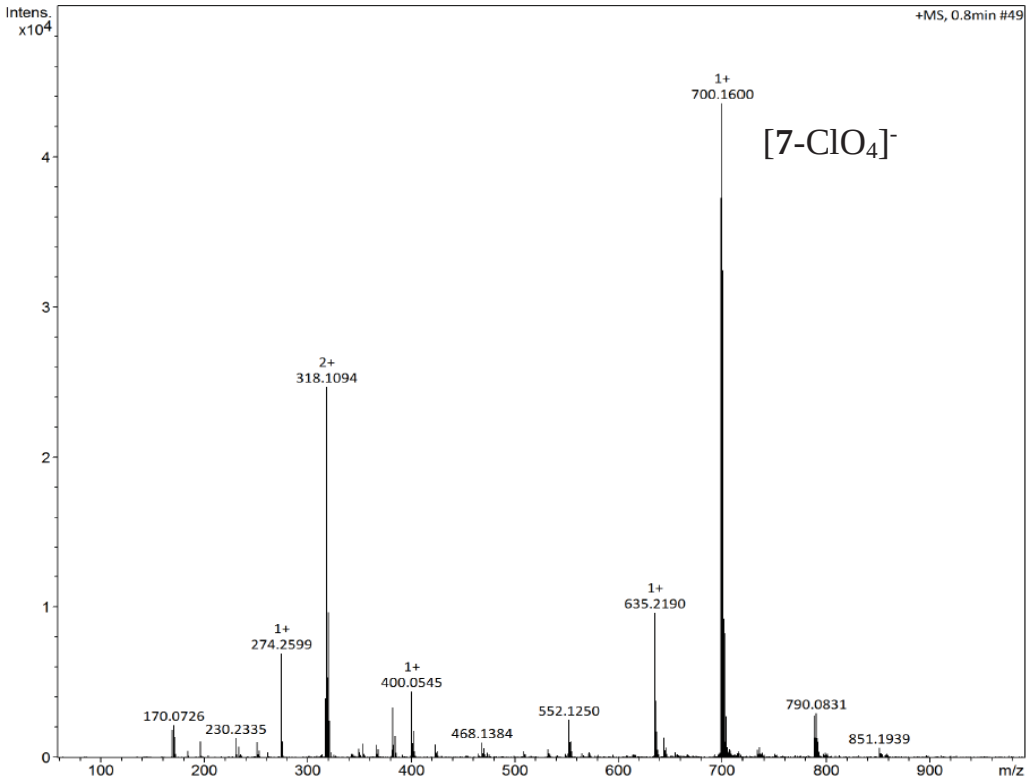

Figure S44. HRMS spectrum of complex **7.**

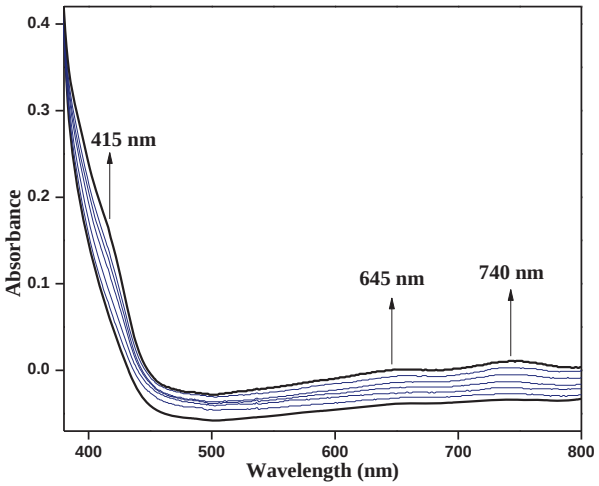

Figure S45. Oxidation of ABTS during spontaneous reduction.

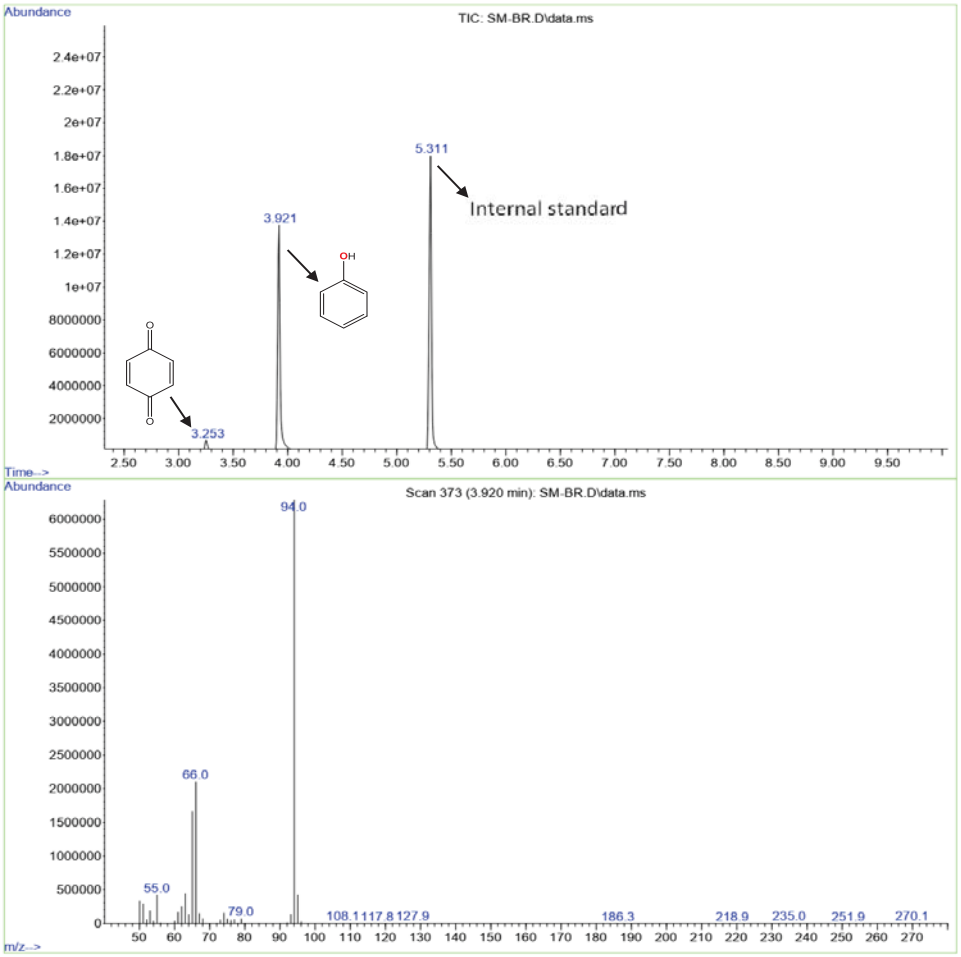

Figure S46. GC-MS profile for the formation of phenol using catalyst **7** and in presence of nitrobenzene as an internal standard.

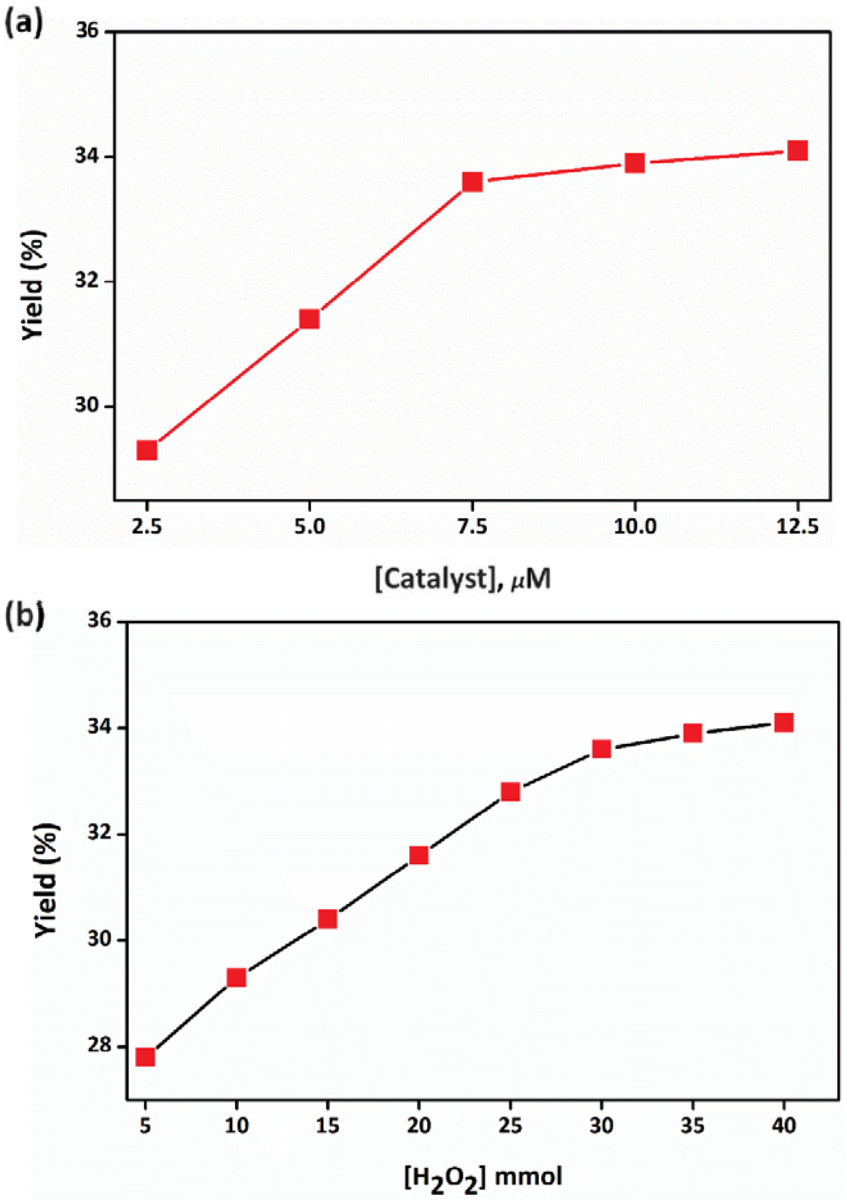

Figure S47. (a) The plot of yield versus various concentration of complex. **(b)** H_2O_2 dependent on the yield of phenol.

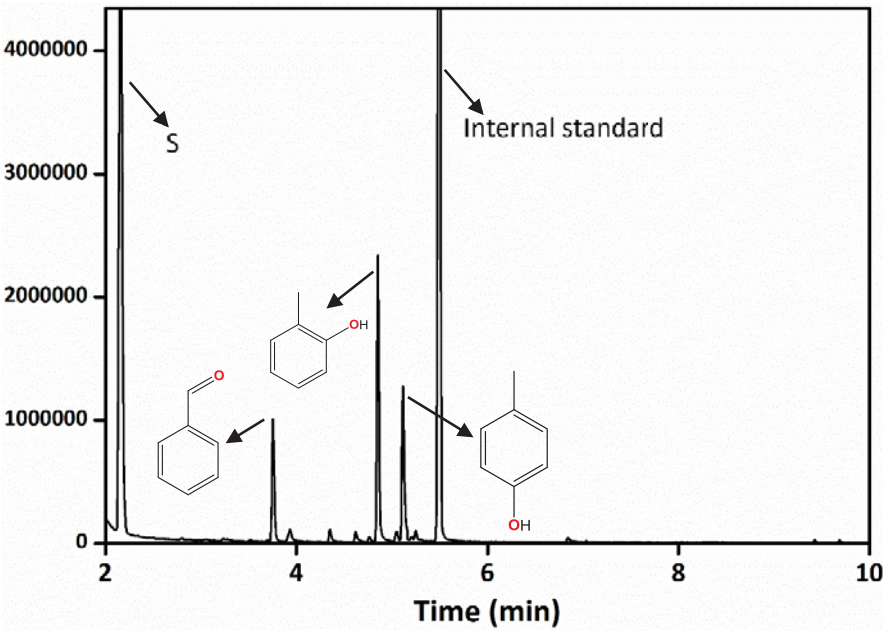

Figure S48. GC trace for the oxidation of toluene using catalyst **7**.

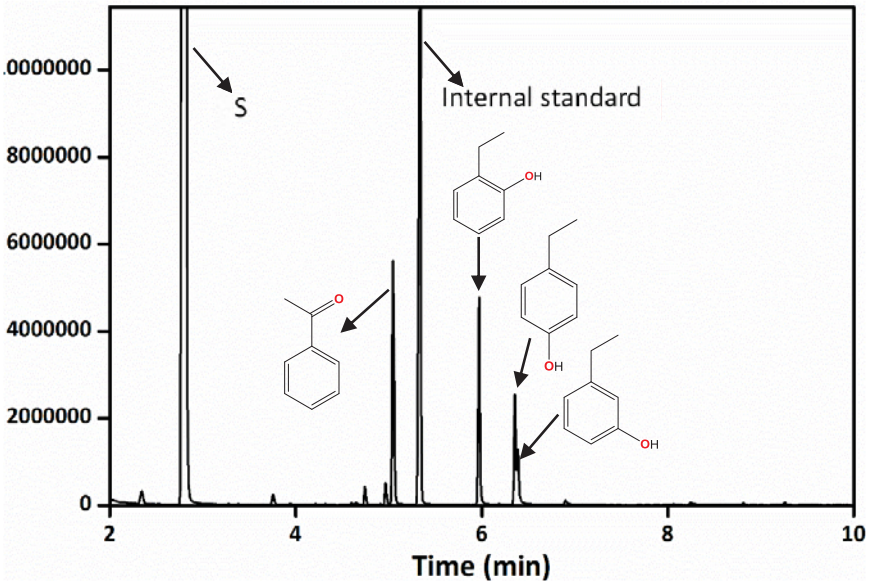

Figure S49. GC trace for the oxidation of ethylbenzene using catalyst **7**.

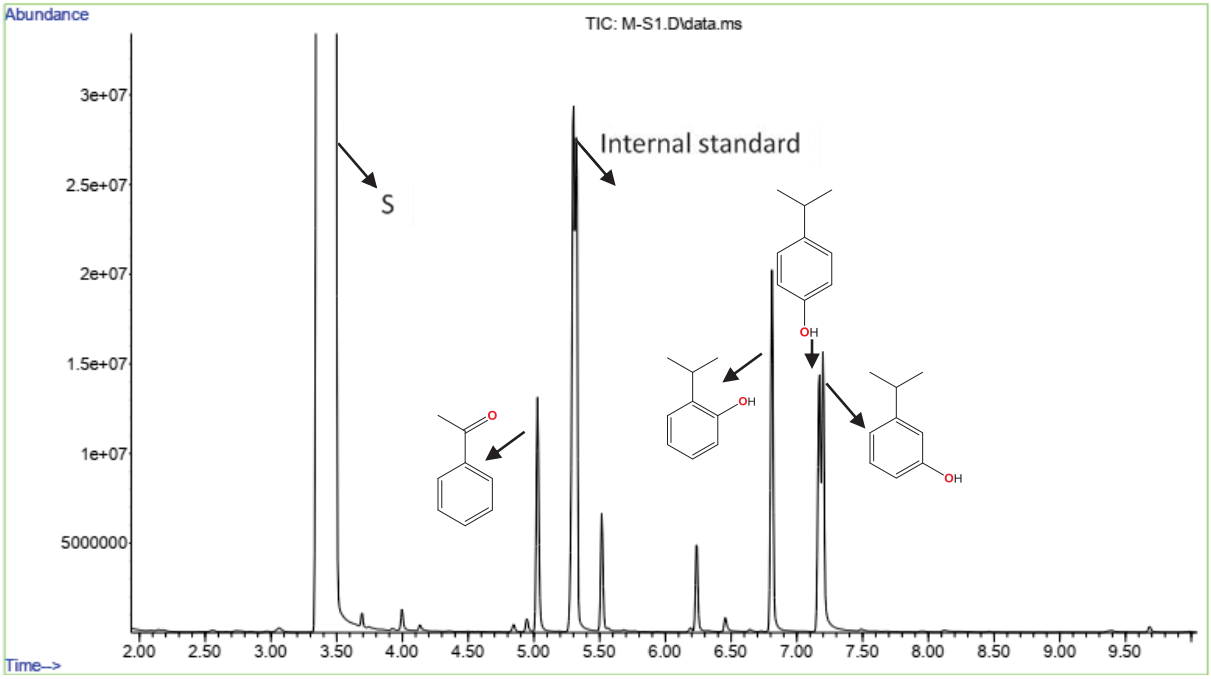

Figure S50. GC trace for the oxidation of cumene using catalyst **7**.

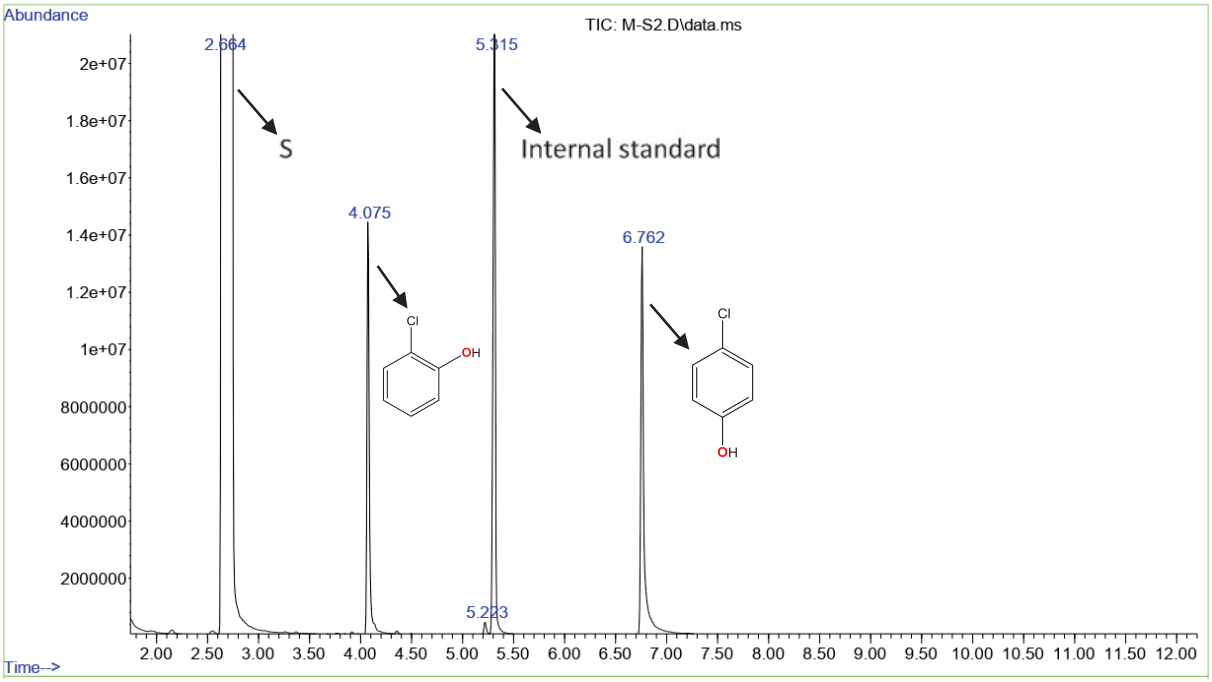

Figure S51. GC trace for the oxidation of chlorobenzene using catalyst **7**.

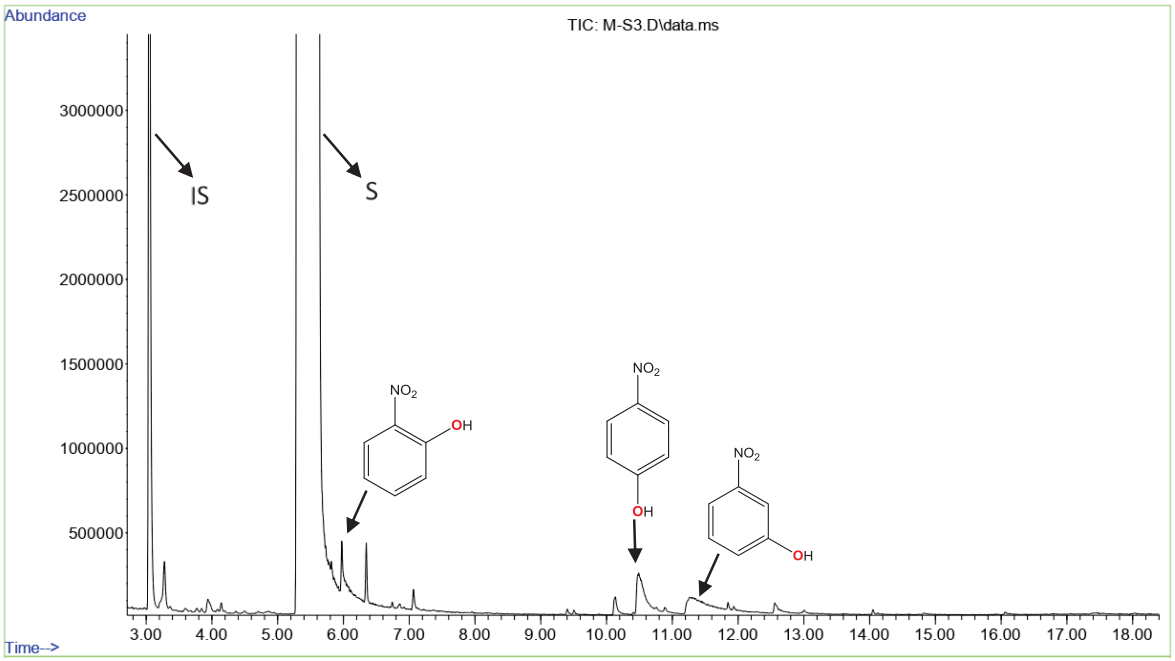

Figure S52. GC trace for the oxidation of nitrobenzene using catalyst **7**.

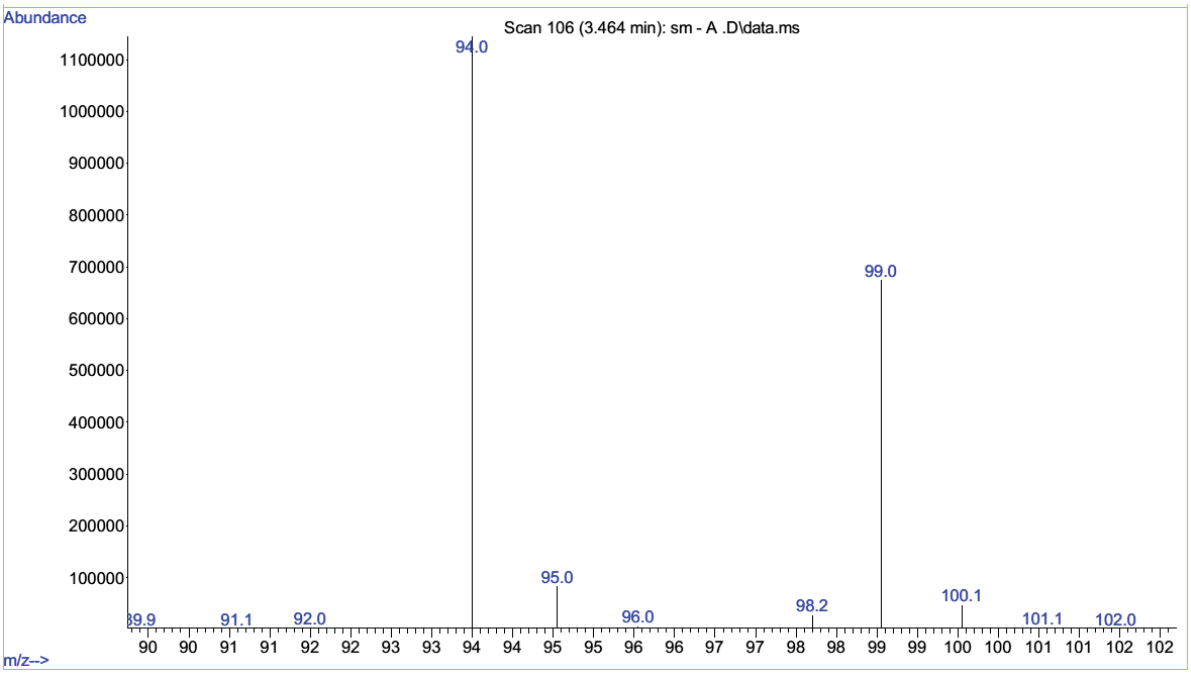

Figure S53. GC-MS profile for the measurement of KIE using C_6H_6 and C_6D_6 and **7** is employed as catalyst.

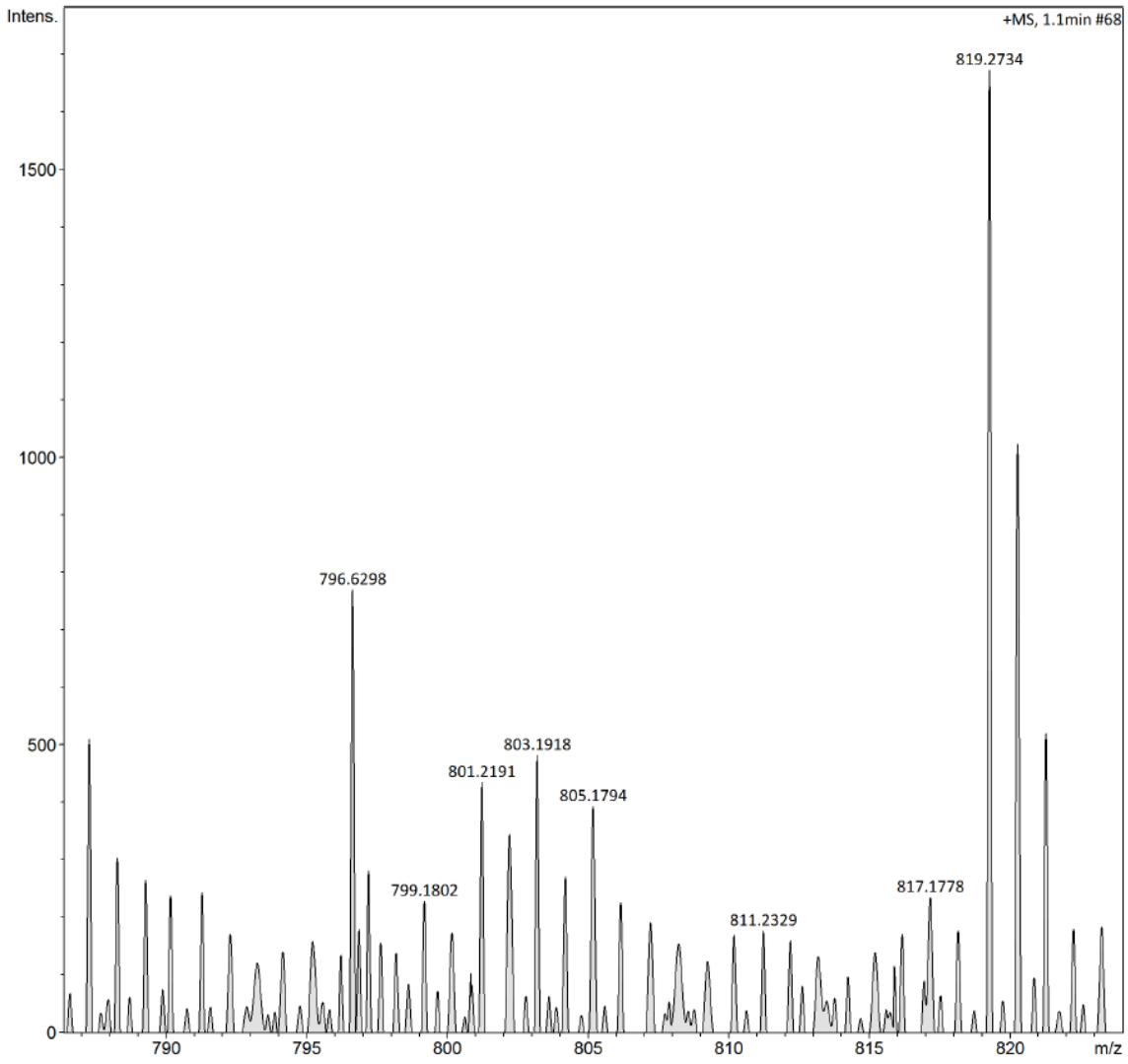

Figure S54. HRMS spectrum of the formation of Cu(II)-species.

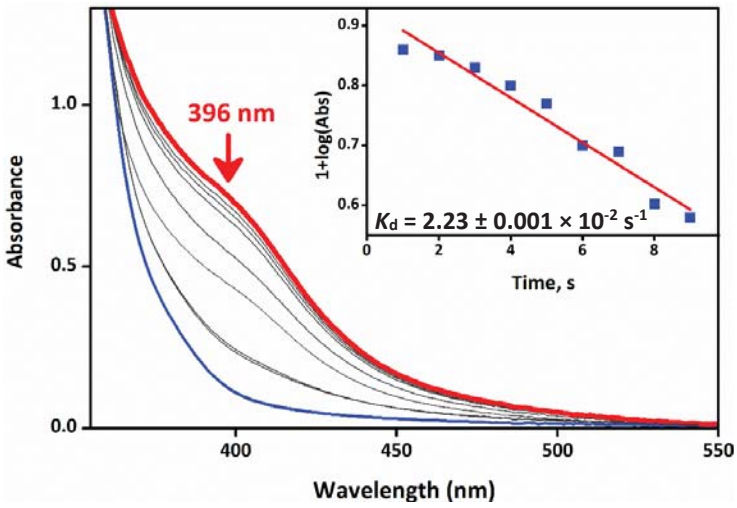

Figure S55. The electronic spectral changes for the reaction of **1** with 10 equivalents of H_2O_2 and 2 equivalents of Et_3N in acetonitrile at -40 °C.

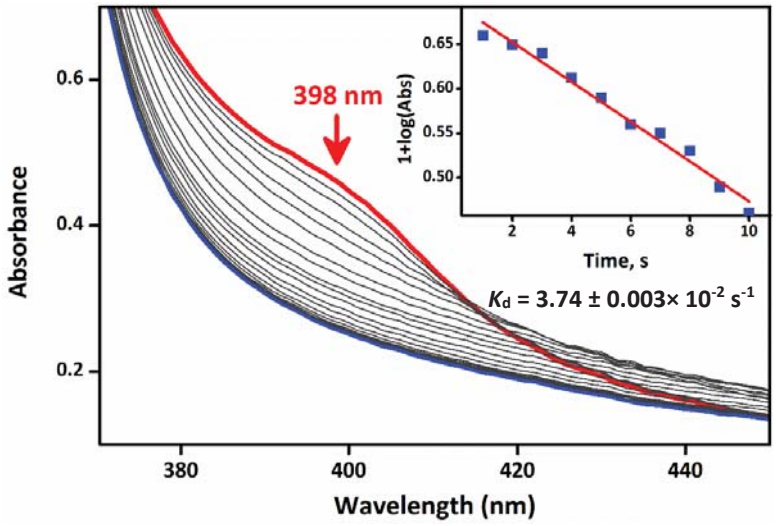

Figure S56. The electronic spectral changes for the reaction of **2** with 10 equivalents of H_2O_2 and 2 equivalents of Et_3N in acetonitrile at -40 °C.

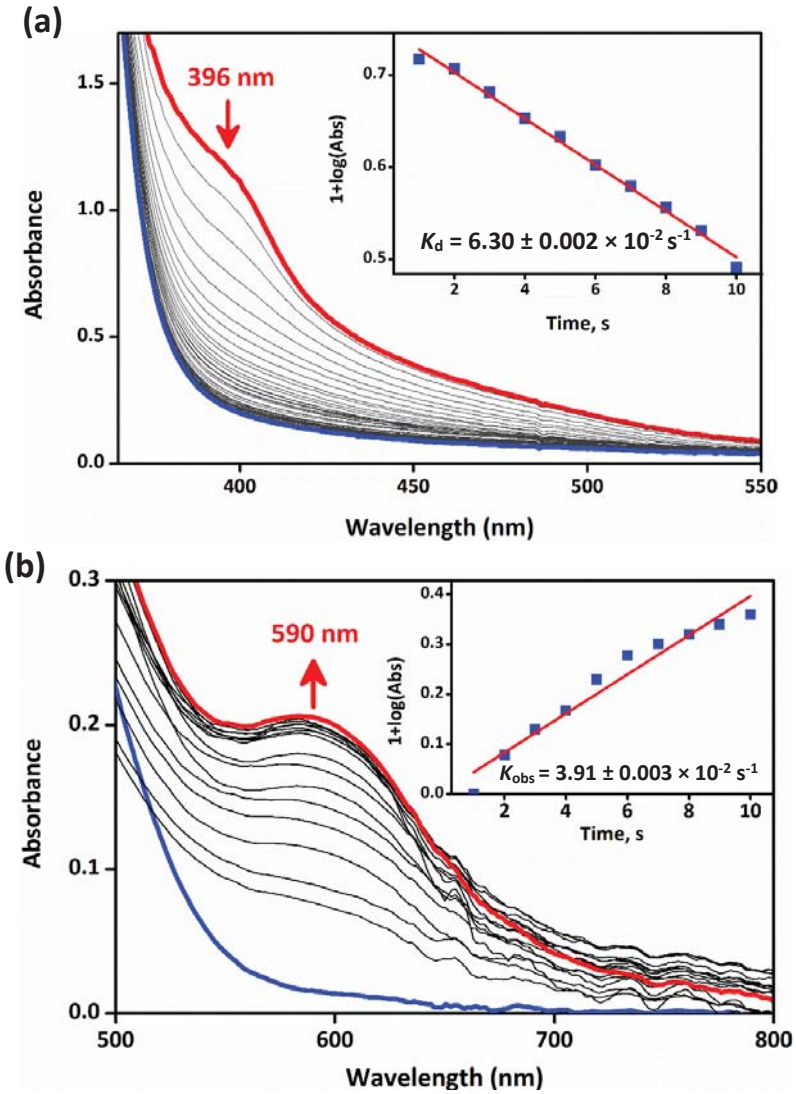

Figure S57. The electronic spectral changes for the reaction of **4** with 10 equivalents of H_2O_2 and 2 equivalents of Et_3N in acetonitrile at -40 °C.

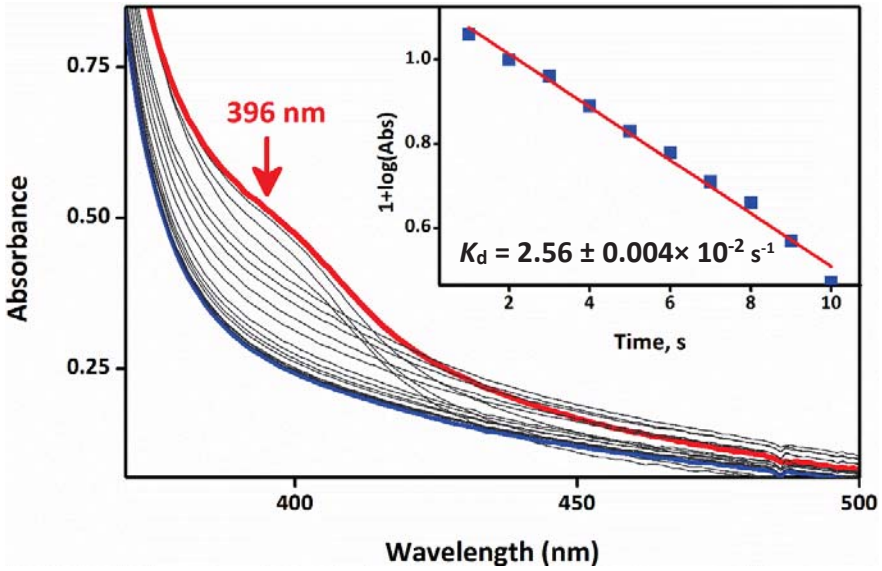

Figure S58. The electronic spectral changes for the reaction of **5** with 10 equivalents of H_2O_2 and 2 equivalents of Et_3N in acetonitrile at -40 °C.

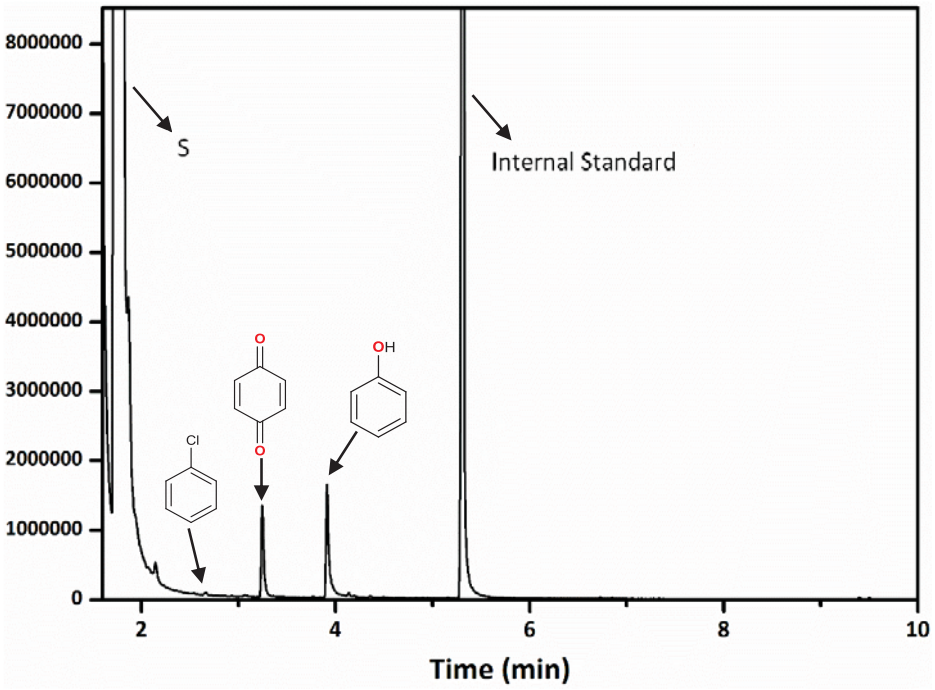

Figure S59. GC trace of the benzene hydroxylation reaction in the presence of CCl_4 as additive using catalyst **7**.

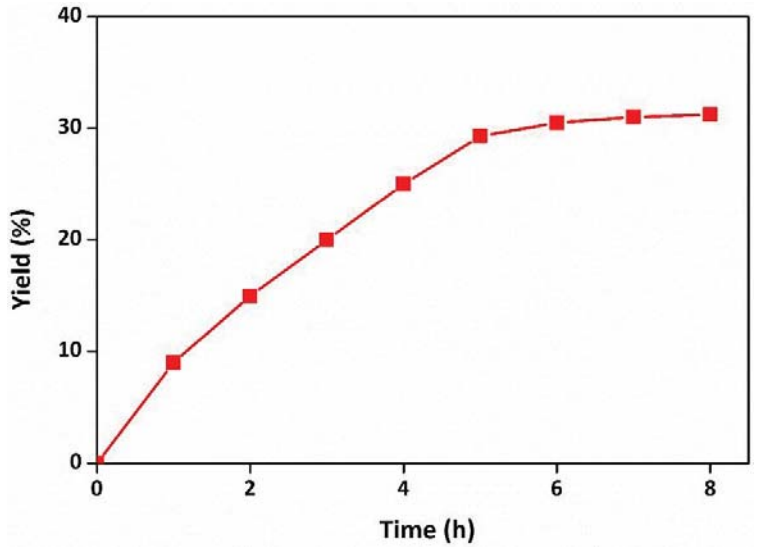

Figure S60. Time depended phenol formation by **7**. Reaction condition: benzene (5 mmol), **7** (2.5 μmol, 0.05%) and triethylamine (2.5 μmol), hydrogen peroxide (30%) (10 mmol) in acetonitrile at 60 °C.

Table S1. NMR, IR and UV-Visible data of ligands (L^1-L^7).

Ligands	^{1}H NMR data (ppm)	^{13}C NMR data (ppm)	IR (KBr disk, υmax / cm^{-1}):	UV-Vis (Acetonitrile; λmax/nm (ε, M^{-1} cm^{-1}))
L^1	^{1}H NMR (400 MHz, $CDCl_3$): δ 8.19 (d, *J*= 8.0 Hz, 1H), 7.68(d, *J*= 8.0 Hz, 2H), 7.55-7.34 (m, 4H), 7.19-7.06 (m, 6H), 6.99-6.85 (m, 5H), 6.79(t, 1H).	^{13}C NMR (100 MHz, $CDCl_3$): δ 165.61, 159.24, 145.33, 138.31, 136.84, 130.03, 128.51, 128.44, 128.30, 128.11, 127.85, 126.33, 116.16, 111.31.	1576 ($\upsilon_{C=N}$)	250(108000), 360(32000)
L^2	^{1}H NMR (400 MHz, $CDCl_3$): δ 8.16 (d, *J*=8.0Hz, 1H), 7.80 (d, *J*=8.0Hz, 1H), 7.66-7.61(m, 6H), 7.51 (t, 1H), 7.40-7.29 (m, 5H), 6.82(t, 1H).	^{13}C NMR (100 MHz, $CDCl_3$): δ 158.33, 147.45, 138.67, 137.56, 135.57, 130.41, 129.88, 128.63, 126.57, 115.86, 109.74.	1583 ($\upsilon_{CH=N}$),	230 (124000), 327(168000)

L^3	^{1}H NMR (400 MHz, $CDCl_3$): δ 8.15 (s, 1H), 7.73(d, *J*= 8.0 Hz, 1H), 7.68-7.47 (m, 6H), 7.33-7.17 (m, 4H), 6.83-6.80 (m, 2H).	^{13}C NMR (100 MHz, $CDCl_3$): δ 158.20, 147.56, 138.54, 137.55, 134.16, 130.45, 128.77, 128.70, 127.67, 116.10, 116.08, 109.71.	1588 ($\upsilon_{CH=N}$),	235(130000), 335(164000)
L^4	^{1}H NMR (400 MHz, $CDCl_3$): δ 8.17 (d, *J*=4.0, 1H), 7.79 (d, *J*=8.0, 1H), 7.72-7.62 (m, 6H), 7.54 (m, 1H), 7.32 (dd, *J*= 8.0Hz, 2H), 6.95 (d, *J*=8.0Hz, 2H), 6.83 (m, 1H), 3.89 (s, 3H).	^{13}C NMR (100 MHz, $CDCl_3$): δ 160.07, 158.41, 147.43, 138.82, 137.51, 137.40, 130.31, 129.95, 128.43, 128.36, 127.87, 121.72, 115.51, 113.97, 109.52, 55.23.	1584 ($\upsilon_{CH=N}$),	238(104000), 328(176000)
L^5	^{1}H NMR (400 MHz, $CDCl_3$): δ 8.24 (s, 1H), 8.22-8.20(m, 3H), 7.79-7.64 (m, 6H), 7.57-7.53 (m, 1H), 7.30-7.28 (m, 2H), 6.92-6.89 (m, 1H).	^{13}C NMR (100 MHz, $CDCl_3$): δ 157.78, 147.64, 147.15, 141.91, 138.13, 137.73, 134.16, 133.77, 130.54, 129.36, 129.00, 126.70, 123.96, 116.93, 110.05.	1589 ($\upsilon_{CH=N}$),	226(80000), 258(116000), 390(188000)
L^6	^{1}H NMR (400 MHz, $CDCl_3$): δ 8.18 (s, 1H), 7.64-7.52 (m, 8H), 7.31 (d, *J*=8.0Hz, 2H), 6.74 (d, *J*=8.0Hz, 3H), 3.04 (s, 6H).	^{13}C NMR (100 MHz, $CDCl_3$): δ 158.24, 150.69, 147.08, 138.92, 137.32, 130.13, 129.93, 128.15, 127.74, 123.47, 114.96, 111.84, 109.38, 40.11.	1585 ($\upsilon_{CH=N}$)	233(33000), 320(64000), 352(84000)
L^7	^{1}H NMR (400 MHz, $CDCl_3$): δ 8.22 (d, *J*=8.0, 1H), 7.71-7.31(m, 9H), 7.01-6.85 (m, 3H), 4.02 (s, 3H).	^{13}C NMR (100 MHz, $CDCl_3$): δ 157.80, 152.11, 146.99, 146.88, 138.59, 137.80, 130.44, 129.93, 128.63, 127.84, 121.47, 115.49, 114.32, 109.62, 107.80, 55.97.	1589 ($\upsilon_{CH=N}$)	240(104000), 334(182000)

Table S2. Bond parameters of complex **1**.

Bond distances (Å)		Bond Angles (°)	
Cu(1)-N(1)	1.9760(17)	N(1)-Cu(1)-N(3)	79.99(7)
Cu(1)-N(3)	2.0797(17)	N(6)-Cu(1)-N(4)	80.04(7)
Cu(1)-N(4)	1.9660(17)	N(1)-Cu(1)-N(4)	143.85(7)
Cu(1)-N(6)	2.0945(17)	N(3)-Cu(1)-N(6)	127.94(7)
N(2)-N(3)	1.413(2)	N(5)-N(6)-Cu(1)	110.05(12)
N(5)-N(6)	1.418(2)	N(2)-N(3)-Cu(1)	110.78(12)

Table S3. Crystal data of complex **1**.

	Complex 1
Empirical formula	**C48 H38 Cl Cu N6 O4**
Formula weight ($gmol^{-1}$)	**861.84**
Space group	**P 21/n**
Temperature /K	**293**
λ (Å) (Mo-Kα)	**0.71073**
Crystal system	**Monoclinic**
a (Å)	**12.3221(3)**
b (Å)	**18.2014(6)**
c (Å)	**18.6062(6)**
α(°)	**90.00**
γ (°)	**90.00**
β(°)	**97.754(3)**
V ($Å^3$)	**4134.8(2)**
Z	**4**
ρ_{calc}(gcm^{-3})	**1.385**
Crystal size (mm)	**0.23x 0.23x 0.23**
F(000)	**1784**
Theta range for data collection	**3.37−25.242**
Index ranges	**−17<h < 17, −25<k <25, −25<l <25.**
Data/restraints/parameters	**10504/0/541**
GOF[a] on F^2	**1.016**
R1[b] [I > 2σ(I)]	**0.0507**
R1[all data]	**0.0823**
wR2[c] [I > 2σ(I)]	**0.1107**
wR2 [all data]	**0.1241**

[a]$GOF = [\Sigma[w(F_o^2 - F_c^2)^2] / M - N]^{1/2}$ (M = number of reflections, N = number of parameters refined). [b]$R1 = \Sigma \| F_o | - | F_c \| / \Sigma | F_o |$. [c]$wR2 = [\Sigma[w(F_o^2 - F_c^2)^2] / \Sigma [(F_o^2)^2]]^{1/2}$.

Table S4. Redox data of **1-7**.

Complex	E_{pc} (V)	E_{pa} (V)	ΔE (mV)	$E_{1/2}$
1	0.302	0.224	78	0.263
2	0.266	0.165	101	0.216
3	0.252	0.123	129	0.188
4	0.265	0.139	126	0.202
5	0.371	0.265	106	0.318
6	0.183	0.099	84	0.141
7	0.223	0.035	188	0.129

Concentration: 1×10^{-3} M in acetonitrile. Supporting electrolyte: 0.1 M TBAP; Reference electrode: Ag/Ag^{+}; working electrode: Pt-sphere; Counter electrode: Pt wire; Scan rate: 100 mV s^{-1}.

Table S5. Optimization of benzene hydroxylation by **7**.

S.No	[Catalyst] (mol %)	Oxidant (mmol)	Temp. (°C)	Conversion (%)	Yield (%)	Selectivity (%)
1	0.025	5	RT	9.9	9.8	>99
2	0.05	5	RT	16.4	16.3	>99
3	0.05	5	60	28	27.8	>99
4	0.05	10	60	29.8	29.3	98
5	0.05	15	60	35.3	30.4	99

Reaction conditions: Benzene (0.4 mL, 5 mmol), catalytic amount of complex **7**, triethylamine (2.5 μmol), hydrogen peroxide (30%) (1.0 mL, 10 mmol) in acetonitrile at 5 hours.